



Cite this: *Environ. Sci.: Nano*, 2019, 6, 834

## Efficient removal of both antimonite (Sb(III)) and antimonate (Sb(V)) from environmental water using titanate nanotubes and nanoparticles†

Tianhui Zhao,<sup>ab</sup> Zhi Tang,<sup>a</sup> Xiaoli Zhao,<sup>\*a</sup> Hua Zhang,<sup>a</sup> Junyu Wang,<sup>ab</sup> Fengchang Wu,<sup>a</sup> John P. Giesy<sup>c</sup> and Jia Shi<sup>d</sup>

Increasing attention has been focused on antimony (Sb) pollution and remediation in aquatic ecosystems, where efficient removal technologies for Sb compounds, particularly Sb(III) and Sb(V), from environmental water are urgently needed. Thus, herein, a mesoporous material, titanate nanotubes (3 nm, TiO<sub>2</sub> NTs) with a large surface area was synthesized and used to remove both Sb(III) and Sb(V) from various natural waters. Furthermore, it was characterized *via* adsorption isotherm and kinetic experiments, and its mechanisms were investigated using various techniques, including Fourier transform infrared spectroscopy (FTIR), X-ray photoelectron spectroscopy (XPS), X-ray diffraction (XRD) and density functional theory (DFT) models. The results show that the maximum amounts of Sb(III) and Sb(V) adsorbed on the TiO<sub>2</sub> NTs (250.0 mg g<sup>-1</sup> and 56.3 mg g<sup>-1</sup>) were due to electrostatic interactions and complexation, which were 20- and 7-fold greater than that on TiO<sub>2</sub> NPs of 12.0 mg g<sup>-1</sup> and 8.6 mg g<sup>-1</sup>, respectively. The removal efficiencies for the TiO<sub>2</sub> NMs using tap water, natural surface water and wastewater were satisfactory, which were nearly 100% for Sb(III) and 100%, 98% and 56%, respectively, for Sb(V) with 5 mg/50 mL TiO<sub>2</sub> and spiked with Sb (200 μg L<sup>-1</sup>). The TiO<sub>2</sub> NTs showed excellent reusability with 0.5 mol L<sup>-1</sup> sodium hydroxide as a desorbing agent. The FTIR and XPS results suggested that the hydroxyl groups play a significant role in the adsorption processes. Based on DFT calculations, it was found that Sb(III) preferred to form O–Ti bonds, Sb(V) formed O–Ti bonds on the {101} facet of the anatase TiO<sub>2</sub> NPs, and Sb(V) preferred to adsorb on the {001} facet. However, for Sb(III), there was no preference between the {101} and {001} facets. This study demonstrates that TiO<sub>2</sub> NTs are promising, easily synthesizable and environmentally friendly adsorbents for both Sb(III) and Sb(V), and can be potentially applied in wastewater treatment.

Received 9th August 2018,  
Accepted 13th January 2019

DOI: 10.1039/c8en00869h

rsc.li/es-nano

### Environmental significance

A mesoporous material, titanate nanotubes (TiO<sub>2</sub> NTs), with large surface areas (175.06 m<sup>2</sup> g<sup>-1</sup>) and pore size diameters (3 nm) was synthesized and used to remove Sb(III) and Sb(V) from environmental water. The interfacial properties of TiO<sub>2</sub> NMs-Sb were characterized *via* FTIR, XPS and EDX spectroscopy. The application of the TiO<sub>2</sub> NMs was demonstrated using tap water, natural surface water and wastewater treatment plant effluent samples spiked with Sb. Moreover, the adsorption of Sb(III) and Sb(V) on TiO<sub>2</sub> NMs was systemically studied, and DFT was used to simulate the adsorption of Sb(III) and Sb(V) on the surfaces of TiO<sub>2</sub> {101} nanoparticles.

## 1. Introduction

Antimony (Sb) is considered a ubiquitous contaminant of global concern. Water contaminated with Sb is hazardous to

both humans and wildlife. Exposures to compounds containing Sb often results in adverse health effects on humans, including damage to the liver and kidneys, dizziness, headaches, vomiting and Adams–Stokes syndrome.<sup>1</sup> Furthermore, prolonged exposure to Sb damages DNA in hamster cells and human hematopoietic cells.<sup>2,3</sup> Since Sb and its compounds have been classified as priority pollutants by the United States Environmental Protection Agency (USEPA) and the European Environment Agency, which have defined the maximum concentration of Sb as 6 μg L<sup>-1</sup> in drinking water,<sup>4</sup> there has been increased attention for the removal of Sb during general wastewater treatment.

<sup>a</sup> State Key Laboratory of Environmental Criteria and Risk Assessment, Chinese Research Academy of Environmental Sciences, Beijing 100012, China.

E-mail: zhaoxiaoli\_zxl@126.com

<sup>b</sup> College of Water Sciences, Beijing Normal University, Beijing 100875, China

<sup>c</sup> Department of Veterinary Biomedical Sciences and Toxicology Centre, University of Saskatchewan, Saskatoon, Saskatchewan, Canada

<sup>d</sup> University of Science and Technology, Beijing, 100083, China

† Electronic supplementary information (ESI) available. See DOI: 10.1039/c8en00869h

China has the world's largest reserves of Sb, and is the largest producer of Sb. Among the major antimony resource countries, China is way ahead in output with an average annual output of about 100 000 tons. In 2017, China's antimony output accounted for 73 percent of the global production. In China, the maximum admissible concentration of Sb in drinking water is  $5 \mu\text{g L}^{-1}$ , and the recommended concentration in Japan is less than  $2 \mu\text{g L}^{-1}$ . For China, the concentration of Sb is mostly less than  $1.00 \mu\text{g L}^{-1}$  in unpolluted water. However, its concentration can be substantially elevated to as much as  $100 \mu\text{g L}^{-1}$  in the vicinity of anthropogenic sources.<sup>5</sup> Moreover, some accidents can also cause serious Sb pollution, such as an emergency contamination issue caused by leakage from a tailings pond that resulted in contamination of the Jialing River in 2015. Therefore, to protect the health of humans and the ecosystem, safe and efficient methods for the removal of Sb compounds from environmental waters, especially drinking water are urgently needed.

The mobilization, fate and risks posed by Sb depend on its oxidation state,<sup>6</sup> which varies in natural aquatic environments, including trivalent (Sb(III)) and pentavalent (Sb(V)). Sb(V) predominately exists as  $\text{Sb(OH)}_6^-$  under oxic conditions, which forms oxides ( $\text{Sb}_2\text{O}_5$ ) that are more soluble than the oxides of Sb(III) ( $\text{Sb}_2\text{O}_3$ ).<sup>7</sup> A significant proportion of Sb(III) occurs as  $\text{Sb(OH)}_3$ , which is more stable under anoxic conditions. This is in contrast with the predictions of thermodynamic equilibrium models based on theoretical physical-chemical properties and discrepancies are often attributed to biological activity and kinetic effects. The toxicity of Sb(III) is 10-fold greater than that of Sb(V).<sup>8</sup> Therefore, researches have focused on efficiently reducing the risks of Sb compounds in aquatic environments. A variety of technologies have been developed to remove Sb and its compounds or accelerate the conversion of Sb(III) into Sb(V), which is less toxic. These techniques primarily include adsorption, coagulation/precipitation and ion-exchange.<sup>9–12</sup> Coagulation/precipitation and ion-exchange usually require the addition of coagulants and several adjustments in pH, and the process can generate large quantities of secondary pollutants that is hazardous to the environment.<sup>13</sup> Adsorption is one of the most promising technologies widely applied due to its simplicity, safety and efficiency.<sup>14</sup>

A range of factors can affect the adsorption of Sb in solution, including pH, temperature, ionic strength and organic matter.<sup>15</sup> Several studies have investigated the use of various adsorbents for the removal of Sb(III) and Sb(V), including graphene,<sup>16</sup> carbon nanofibers decorated with zirconium oxide ( $\text{ZrO}_2$ ),<sup>4</sup> nanoscale zero-valent iron,<sup>17</sup>  $\alpha\text{-FeOOH}$ ,<sup>18</sup>  $\alpha\text{-MnO}_2$  (ref. 19) and bio-adsorbents.<sup>20</sup> However, the adsorption amounts by these adsorbents are relatively small and there are other limitations, such as long equilibrium times, requirement of additional chemicals and complex regeneration process. Some of the novel adsorbents, such as Zr-MOFs<sup>21</sup> and reduced graphene oxides/ $\text{Mn}_3\text{O}_4$ ,<sup>22</sup> have a large adsorption amount due to their large specific surface areas and/or porous structures, which show that metal nano-materials

have great potential in Sb removal. Therefore, developing novel adsorbents with greater adsorption capacity and chemical stability is an urgent need for the remediation of Sb-contaminated sites.<sup>15,23,24</sup>

Among the materials used to remove inorganic contaminants,  $\text{TiO}_2$  nano-materials ( $\text{TiO}_2$  NMs) have drawn considerable attention for removing multiple metals including  $\text{Cu}^{2+}$ ,  $\text{Hg}^{2+}$ ,  $\text{Cd}^{2+}$ ,  $\text{Pb}^{2+}$ ,  $\text{As}^{3+}$  and  $\text{As}^{5+}$ , each of which has advantages.<sup>25–30</sup> However, the simultaneous removal of both Sb(III) and Sb(V) using  $\text{TiO}_2$  NMs has been rarely reported. The adsorption of Sb by nano  $\text{TiO}_2$  and cross-linked chitosan has been studied,<sup>31</sup> while the adsorption of radioactive Sb by titania was also reported.<sup>32</sup> The adsorption capacities of nano-materials depend on their surface areas, structures, density of active sites and functional groups.<sup>33,34</sup> Compared with particles, nanotubes have greater surface areas and more mesopores and functional groups, and it has been reported that nanotubes have greater adsorption capacity and efficiency compared to particles of the same materials in the bulk form.<sup>35–37</sup> However, due to the lower availability of  $\text{TiO}_2$  nanotubes ( $\text{TiO}_2$  NTs), there are few reports on the use of  $\text{TiO}_2$  NTs for the simultaneous removal of both Sb(III) and Sb(V). Compared with other nanomaterial adsorbents for the removal of Sb,  $\text{TiO}_2$  NTs are relatively easily synthesized and are considered environmentally friendly, which make them suitable for large-scale industrial production and wide-spread application. Furthermore, the sorption of Sb on  $\text{TiO}_2$  NMs has rarely been investigated, and there are limited reports on the use of density functional theory (DFT) to illustrate the interaction mechanism of  $\text{Sb(OH)}_6^-$  and  $\text{Sb(OH)}_3$  on the surfaces of  $\text{TiO}_2$  NMs.

In the present study,  $\text{TiO}_2$  NTs, prepared by hydrothermal synthesis, were used to simultaneously remove the two oxidation states of Sb. The effects of pH on the efficiency of the removal of Sb were determined, and adsorption isotherm and kinetics experiments were performed. Adsorption isotherm experiments and dynamic modeling were performed to understand the adsorption behaviors of the samples. Two materials,  $\text{TiO}_2$  NMs ( $\text{TiO}_2$  NPs and  $\text{TiO}_2$  NTs), were used to simultaneously remove trivalent and pentavalent Sb in three natural water samples. Furthermore, the possible adsorption mechanisms were investigated *via* X-ray diffraction (XRD), Fourier transform IR (FTIR) spectroscopy, X-ray photoelectron spectroscopy (XPS) and DFT calculations.

## 2. Materials and methods

### 2.1 Reagents and materials

All chemicals and reagents used in this study were of analytical grade or greater purity. The water (ultrapure water,  $18.2 \text{ M}\Omega \text{ cm}$ ) used in all experiments was prepared using a Milli-Q SP reagent water system (Millipore, Bedford, MA).  $\text{C}_8\text{H}_4\text{K}_2\text{O}_{12}\text{Sb}_2 \cdot x\text{H}_2\text{O}$  and  $\text{KSb(OH)}_6$  were purchased from Sigma-Aldrich, which were dissolved in deionized (DI) water to prepare Sb(III) and Sb(V) stock solutions, respectively.  $\text{TiO}_2$  NPs were purchased from J&K Scientific Ltd. (25–50 nm,

average surface area  $19.6 \text{ m}^2 \text{ g}^{-1}$ ). For the natural water experiments, tap water was collected from the Beijing District, surface water from the Olympic Park in Beijing and domestic treatment plant effluent from the South Dagang Sewage Treatment Plant.

## 2.2 Preparation of protonated $\text{TiO}_2$ NTs

$\text{TiO}_2$  NTs were prepared *via* the alkaline hydrothermal method.<sup>36</sup> The surface area and pore diameters of the  $\text{TiO}_2$  NTs were controlled by varying the reaction temperature and contact time of the  $\text{TiO}_2$  NPs with 10 M NaOH solution. First, 3 g of anatase-phase  $\text{TiO}_2$  NPs powder was dispersed in 100 mL of 10 M NaOH solution and vigorously stirred for 24 h. Subsequently, the mixture was autoclaved at  $150 \text{ }^\circ\text{C}$  for 24 h. The obtained white product was washed with DI water until the supernatant pH became neutral, and then soaked in 0.5 M hydrochloric solution for 5 h. Interlayer sodium ions were anticipated to be exchanged for protons during the soaking of the nanotubes in acidic solution. Then, the protonated  $\text{TiO}_2$  NTs were again washed to pH 7 with deionized water. Finally, the products were dried at  $90 \text{ }^\circ\text{C}$ .

## 2.3 Characterization of $\text{TiO}_2$ NMs before and after adsorption

Transmission electron microscopy (TEM) images were recorded on an H7500 transmission electron microscope (Hitachi, Japan) operating at 120 kV. The specific surface areas (BET) of the samples were investigated using an F-Sorb 3400 automatic surface area Gold APP Instrument. Zeta potentials were determined using a Nano-ZS90 Zetasizer (Malvern, United Kingdom). The morphologies of the adsorbents were examined using a scanning electron microscope (LEO 1530 field-emission SEM) and energy dispersive X-ray spectroscopy (EDX), with dedicated software. X-ray diffraction (XRD) analysis (PAN'alytical X'Pert Alpha 1, using Cu K- $\alpha$ 1,  $\lambda = 1.5406 \text{ \AA}$ ) was performed to analyze the crystal structure of the  $\text{TiO}_2$  NPs and  $\text{TiO}_2$  NTs.

## 2.4 Batch experiments

All batch tests were performed in 100 mL glass bottles by adding 5 mg (dry mass) of  $\text{TiO}_2$  NP or  $\text{TiO}_2$  NT adsorbent to 50 mL of Sb solution. The ionic strength was controlled to 0.02 M with 1 M NaCl solution. The mixture was sealed and shaken at 220 rpm for 6 h. After shaking the sample, the supernatant was filtered through  $0.45 \text{ }\mu\text{m}$  pore-size cellulose acetate membrane filters and the residual concentrations of Sb(III) and Sb(V) in the filtrate were simultaneously quantified *via* HPLC-HG-atomic fluorescence spectrophotometry.

**2.4.1 Effects of pH.** To evaluate the effects of pH on the adsorption of both Sb(III) and Sb(V), experiments were performed where the initial concentrations of Sb(III) and Sb(V) were constant at  $1 \text{ mg L}^{-1}$ , and the pH of the aqueous solution was varied between 2.0 and 10.0. The solution pH was adjusted using  $0.1 \text{ mol L}^{-1}$  HCl or  $0.1 \text{ mol L}^{-1}$  NaOH.

**2.4.2 Adsorption isotherms and thermodynamics.** Batch experiments of Sb(III) and Sb(V) sorption on adsorbents were

performed by adding 5 mg of adsorbent to 50 mL of Sb(III) or Sb(V) solution at three temperatures ( $15 \text{ }^\circ\text{C}$ ,  $25 \text{ }^\circ\text{C}$  and  $35 \text{ }^\circ\text{C}$ ). Adsorption isotherms were developed for initial concentrations of Sb(III) and Sb(V) in the range of  $0.5\text{--}40.0 \text{ mg L}^{-1}$  and  $0.01\text{--}10.0 \text{ mg L}^{-1}$  at the optimal pH ( $\text{pH} = 2.2 \pm 0.1$ ), respectively. The dosage of adsorbents for all the experiments was  $0.1 \text{ g L}^{-1}$ . To determine the factors that cause the conversion of Sb(III) to Sb(V), the Sb(III) adsorbed on the  $\text{TiO}_2$  NP and  $\text{TiO}_2$  NT surfaces was studied at different pH under sunlight or in the dark. The amount of Sb(III) was  $1 \text{ mg L}^{-1}$ , and studies were conducted with or without  $\text{TiO}_2$  NPs and  $\text{TiO}_2$  NTs.

**2.4.3 Desorption studies.** Desorption thermodynamic properties are important for describing the adsorption properties of sorbents. Desorption experiments were performed using  $0.5 \text{ mol L}^{-1}$  NaOH as the desorbing agent. After the adsorption process described above, the Sb-loaded  $\text{TiO}_2$  NMs were withdrawn and added to NaOH and equilibrated for 12 h at  $15 \text{ }^\circ\text{C}$ ,  $20 \text{ }^\circ\text{C}$ ,  $25 \text{ }^\circ\text{C}$ ,  $30 \text{ }^\circ\text{C}$  or  $35 \text{ }^\circ\text{C}$ . After desorption, the supernatant was filtered through  $0.45 \text{ }\mu\text{m}$  pore-size cellulose acetate membrane filters and the residual concentrations of Sb(III) and Sb(V) in filtrate were quantified *via* HPLC-HG-atomic fluorescence spectrophotometry.

**2.4.4 Adsorption kinetics experiments.** For the kinetic studies, a mixture consisting of  $\text{TiO}_2$  NPs or  $\text{TiO}_2$  NTs and Sb(III) and Sb(V) solution with an initial concentration of  $1 \text{ mg L}^{-1}$  was shaken in the dark for 6 h. Samples were withdrawn at specific intervals and the same methods described above were used to quantify the residual concentration in the filtrates.

**2.4.5 Adsorption experiments in natural water.** To test performance of the  $\text{TiO}_2$  NMs for the removal of Sb from natural water, which has a more complex composition than deionized water, three types of environmental water samples, including tap water, surface water and domestic treatment plant effluent, were investigated. The experiments were conducted in batch mode by adding 5 mg/50 mL  $\text{TiO}_2$  NPs and  $\text{TiO}_2$  NTs to the samples. Samples of natural water were spiked with  $200 \text{ }\mu\text{g L}^{-1}$  Sb(III) or Sb(V) prior to adsorption. The container was a 100 mL polycarbonate bottle and the final volume was 50 mL. Total concentration of organic carbon (TOC) and degree of humification were determined using a Multi N/C 3100 (Germany) spectrometer *via*  $\text{UV}_{465/665}$  visible absorbance (Agilent 8453, the UV absorbance of a given sample determined at 465 nm and 665 nm).

**2.4.6 Reusability experiments.** Reusability is an important factor for an effective adsorbent. Thus, to investigate the adsorption–desorption reliability of the  $\text{TiO}_2$  NPs and  $\text{TiO}_2$  NTs, reusability experiments were carried out using  $0.5 \text{ mol L}^{-1}$  NaOH solution as the desorbing agent. After the adsorption process described above, the Sb(III) or Sb(V)-loaded  $\text{TiO}_2$  NMs were withdrawn, then added to the desorption solution and equilibrated for 6 h. Subsequently, they were washed thoroughly with deionized water, dried under vacuum at  $65 \text{ }^\circ\text{C}$ , and then, the recovered adsorbent was used in the subsequent four-cycle adsorption–desorption experiments.

## 2.5 Fourier transform infrared spectroscopy (FTIR)

FTIR spectra of the TiO<sub>2</sub> NPs and TiO<sub>2</sub> NTs were recorded using a Nicolet Magna-IR 750 FTIR spectrometer (Nicolet Magna-IR 750, Nicolet) with KBr powder as the background in the wavelength range of 400 cm<sup>-1</sup> to 4000 cm<sup>-1</sup> at a resolution of 4 cm<sup>-1</sup> and averaged over 200 scans.

## 2.6 X-ray photoelectron spectroscopy (XPS)

To detect Sb(III) and Sb(V) adsorbed on the surfaces of the adsorbents after the reaction, the samples were freeze-dried and characterized *via* XPS using a PHI Quantera SXM spectrometer equipped with a monochromatic AlK $\alpha$  X-ray source (1486.6 eV, 600 W and 15 kV). A charge neutralizer filament was used during the measurements to compensate for charging of the samples. High-resolution XPS was performed using a 0.1 eV step size and pass energy of 23.5 eV (the depth of the samples analyzed ranged from 8 nm to 10 nm). XPS data processing and peak fitting were performed using a nonlinear least-squares fitting program (XPS peak software 4.1).

## 2.7 Theoretical interatomic sorption analysis by density functional theory (DFT) calculations

Density functional theory (DFT) calculations are a reliable predictive approach to study the quantum properties of materials and provide guidance for the construction of new types of nanostructures. DFT calculations of the optimized structures and molecular adsorption on the TiO<sub>2</sub> {001}, {100} and {101} facets were performed within the generalized gradient approximation (GGA) described by the Perdew–Burke–Ernzerhof (PBE) exchange–correlation function. The electronic-ion interactions of elements were described by projector augmented wave (PAW) with the QUANTUM ESPRESSO code. A cutoff energy of 500 eV was applied. The experimental lattice and structure including slab were optimized by energy minimization. The self-consistent convergence to the tolerance was set to  $1 \times 10^{-6}$  eV  $\text{\AA}^{-1}$ , and the force maximum of total energy convergence was set to 0.02 eV  $\text{\AA}^{-1}$  on atoms. A (4 × 2) supercell of anatase TiO<sub>2</sub> tetragonal crystal system with lattice parameters ( $a = 3.78$   $\text{\AA}$  and  $c = 9.51$   $\text{\AA}$ ) was established. To obtain the total binding energy for each system, the atomic positions were fully relaxed with the volume of the supercell fixed. Three slab models cut from different facets of TiO<sub>2</sub> with 4 layers and vacuum layer of 10  $\text{\AA}$  were constructed on the {001}, {100} and {101} facets. The Monkhorst–Pack scheme with  $2 \times 2 \times 2$   $k$ -points in the Brillouin zone was selected for structure optimization. After the TiO<sub>2</sub> facet optimized, Sb(III) and Sb(V) were added separately to the surface for relaxing the adsorption results.

# 3. Results and discussion

## 3.1 Characterization of TiO<sub>2</sub> NPs and TiO<sub>2</sub> NTs before and after adsorption

**3.1.1 Electron microscopy and specific surface area (BET) analyses.** The TEM images of the TiO<sub>2</sub> NPs and TiO<sub>2</sub> NTs be-

fore and after the adsorption of Sb(III) or Sb(V) are shown in Fig. 1. From the TEM images, it can be seen that the diameters of the TiO<sub>2</sub> NPs are in the range of 25–50 nm, and average surface area is 19.36 m<sup>2</sup> g<sup>-1</sup>. Moreover, the TiO<sub>2</sub> NTs maintained perfect, hollow and well-defined uniformly tubular morphologies, where the outer and inner diameters of the as-prepared TiO<sub>2</sub> NTs were 8 nm to 9 nm and 5 nm to 6 nm, respectively. In addition, the surface area of the TiO<sub>2</sub> NTs (175.06 m<sup>2</sup> g<sup>-1</sup>) is bigger than that of the TiO<sub>2</sub> NPs, which resulted in a greater adsorption capacity of Sb on TiO<sub>2</sub> NTs. After Sb was adsorbed on the surfaces of the TiO<sub>2</sub> NTs and TiO<sub>2</sub> NPs, their morphology changed. Crystalline Sb(V) can be observed in the TEM and SEM images (Fig. 1). This is mainly due to the large amount of Sb adsorbed on the surfaces of the material, which was then crystallized during drying (Fig. 2). The TEM and SEM images also demonstrated that Sb(III) and Sb(V) were strongly adsorbed on surfaces of the TiO<sub>2</sub> NTs and TiO<sub>2</sub> NPs and formed crystalline structures. Energy dispersive spectrometry (EDX) was used to investigate the specific elemental contents before and after Sb(III) and Sb(V) were adsorbed on the TiO<sub>2</sub> NPs and TiO<sub>2</sub> NTs (Fig. S1†). The main elements present in the TiO<sub>2</sub> NPs and TiO<sub>2</sub> NTs (Fig. S1a†) prior to adsorption were carbon, oxygen and titanium, with no Sb. After adsorption, Sb appeared in the elemental analysis (Fig. S1b†), which indicates that was Sb adsorbed on the surfaces of the TiO<sub>2</sub> NPs and TiO<sub>2</sub> NTs.

**3.1.2 The point of zero charge (PZC) of TiO<sub>2</sub> NMs.** The point of zero charge (PZC) of the materials was determined using their zeta potential in solution at various pH (Fig. S2†). The PZC is influenced by the protonation and deprotonation of surface hydroxyl groups.<sup>38</sup> Since there were more deprotonated hydroxyl groups on the surface of the TiO<sub>2</sub> NTs during the synthetic process, the PZC of the TiO<sub>2</sub> NPs (pH = 6.6) was higher than that of the TiO<sub>2</sub> NTs (pH = 3.5).<sup>36</sup>

**3.1.3 XRD spectra.** From the XRD spectra, significant differences were observed between the crystal structures of the TiO<sub>2</sub> NTs and that of the TiO<sub>2</sub> NPs (Fig. 3). Anatase is the dominant phase in the TiO<sub>2</sub> NPs, while it absent in the spectrum of the TiO<sub>2</sub> NTs. The peak at  $2\theta \approx 10^\circ$  for the TiO<sub>2</sub> NTs indicates that interlayers exist.<sup>39,40</sup> As shown in the spectrum of Sb adsorbed on TiO<sub>2</sub> NTs, the intensity of the peak at  $2\theta \approx 10^\circ$  significantly decreased, which indicates that the adsorption of Sb(III) and Sb(V) broke the interlayer structure of the TiO<sub>2</sub> NTs.<sup>30</sup> Peaks at  $2\theta \approx 15^\circ$ ,  $29^\circ$ , and  $32^\circ$ , which mainly represent the adsorption of Sb(V), appear in the spectra of TiO<sub>2</sub> NPs/Sb(V) and TiO<sub>2</sub> NTs/Sb(V).<sup>41</sup> In addition, the disappearance of the characteristic peak of sodium titanate ( $2\theta \approx 28^\circ$ ) indicated that the content of sodium titanate decreased.<sup>42</sup>

## 3.2 Batch experiments

**3.2.1 Effect of pH on the adsorption of Sb(III) and Sb(V).** In aqueous environments, pH is an important factor affecting adsorption,<sup>8,43</sup> which strongly influences the surface charges of TiO<sub>2</sub> NMs and physicochemical properties of Sb. Thus, the

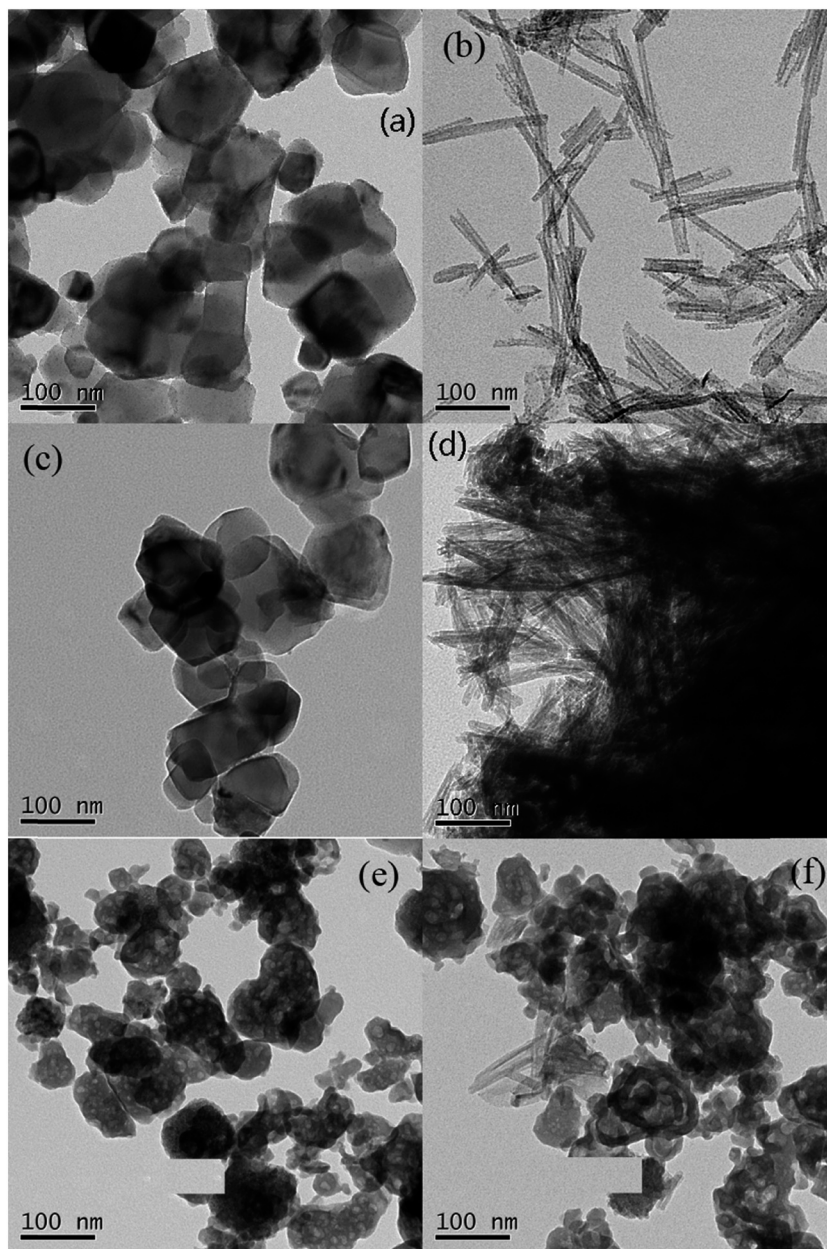


Fig. 1 TEM images of TiO<sub>2</sub> NPs (a), TiO<sub>2</sub> NTs (b), TiO<sub>2</sub> NPs/Sb(III) (c), TiO<sub>2</sub> NTs/Sb(V) (d), TiO<sub>2</sub> NPs/Sb(III) (e) and TiO<sub>2</sub> NTs/Sb(V) (f).

influence of pH on adsorption was explored by varying the pH from 2.0 to 10.0. The TiO<sub>2</sub> NTs exhibited significantly greater adsorption capacity for both Sb(III) and Sb(V) than the TiO<sub>2</sub> NPs (Fig. 4). The efficiency of the adsorption of Sb(III) on both the TiO<sub>2</sub> NTs and TiO<sub>2</sub> NPs was not significantly influenced by the variation in pH from 2.0 to 10.0 (Fig. 4a). The efficiency of adsorption of Sb(III) on the TiO<sub>2</sub> NTs was 99%, which was significantly higher than that of the TiO<sub>2</sub> NPs (41%). Similar results of pH-independent Sb(III) adsorption were reported previously for goethite and amorphous Fe hydroxides as sorbents.<sup>7,44</sup> When the pH was 2.0, the efficiency of the removal of Sb(V) on the TiO<sub>2</sub> NTs and TiO<sub>2</sub> NPs reached the maxima of 95% and 22%, respectively (Fig. 4b). The amount of Sb adsorbed was low at the initial pH of 2.0–

5.0, and even lower at pH 5.0–10.0. When the pH was higher than 4.0, the removal efficiency of Sb(V) was low and inversely proportional to pH. The changes in the zeta potentials of the TiO<sub>2</sub> NPs and TiO<sub>2</sub> NTs before and after Sb(III) and Sb(V) adsorption are shown (Fig. S2†).

In natural water, Sb(III) and Sb(V) generally exist as complexes. The predominant species of aqueous Sb(III) and Sb(V) species are Sb(OH)<sub>3</sub> and Sb(OH)<sub>6</sub><sup>−</sup> in the pH range of 2.0–11.0, respectively.<sup>8</sup> At pH ranging from 2.0–4.0, the surfaces of the TiO<sub>2</sub> NPs and TiO<sub>2</sub> NTs were more positively charged, thus Sb(OH)<sub>6</sub><sup>−</sup> could adsorb on their surfaces through electrostatic interactions and complexation. At higher pH, the surface charges of the TiO<sub>2</sub> NPs and TiO<sub>2</sub> NTs shifted from positive to negative, and the electrostatic adsorption force was

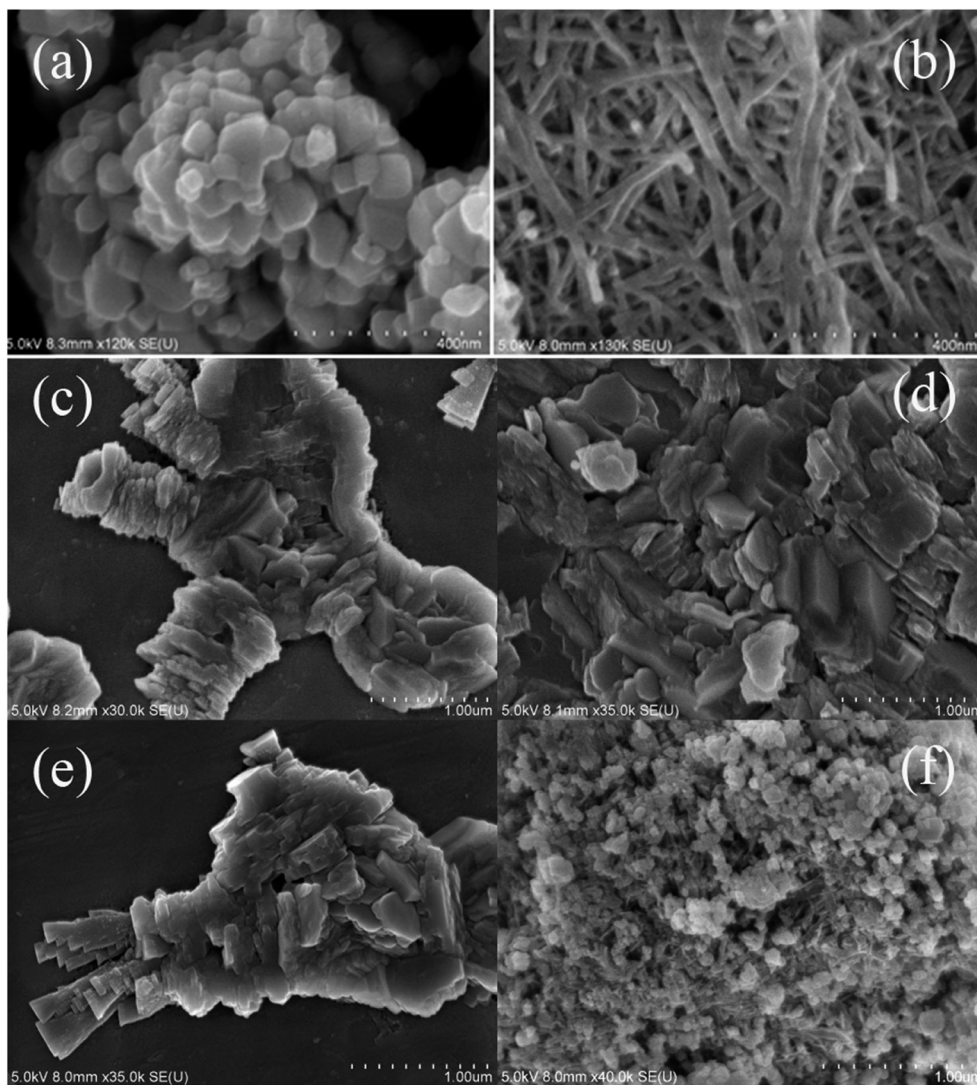


Fig. 2 SEM images of TiO<sub>2</sub> NPs (a), TiO<sub>2</sub> NTs (b), TiO<sub>2</sub> NPs/Sb(III) (c), TiO<sub>2</sub> NTs/Sb(V) (d), TiO<sub>2</sub> NPs/Sb(III) (e) and TiO<sub>2</sub> NTs/Sb(V) (f).

weakened under this circumstance. A previous study indicated the formation of negatively charged inner-sphere Sb(III/V) complexes on TiO<sub>2</sub>.<sup>15</sup> Therefore, the adsorption capacities of Sb(III) on the TiO<sub>2</sub> NPs and TiO<sub>2</sub> NTs fluctuated slightly over a wide pH range, and thus slightly influenced by pH. Moreover, the adsorption efficiency of Sb(V) on the TiO<sub>2</sub> NMs exhibited an evident decrease, which may be due to the hindering effect of electrostatic repulsion, but Sb(V) could also adsorb on TiO<sub>2</sub> NMs through complexation.

Sb(III) may be converted to Sb(V) during adsorption on surfaces of the TiO<sub>2</sub> NPs and TiO<sub>2</sub> NTs (Fig. 5). Sb(V) was determined in aqueous media after adsorption even though it had not been added initially. The concentrations of Sb(V) were directly proportional to pH, and its concentrations in the filtrate after adsorption on the TiO<sub>2</sub> NPs were significantly higher than that for the TiO<sub>2</sub> NTs. The maximum concentration in the filtrate after the adsorption of Sb(V) was 112 μg L<sup>-1</sup>. The concentrations of Sb(V) in the filtrate after adsorption on the TiO<sub>2</sub> NP sample were significantly higher than after adsorption

on the TiO<sub>2</sub> NTs, especially in alkaline solution, and there was no transformation of Sb(III) into Sb(V) in the absence of TiO<sub>2</sub> NPs or TiO<sub>2</sub> NTs both in the dark and under sunlight (Fig. 5).

These results indicate that the conversion of Sb(III) to Sb(V) was caused by the TiO<sub>2</sub> NMs. The limited results from previous studies indicate that this is due to the redox reactions of Sb(III) adsorbed on other metallic oxides in aqueous media.<sup>7,18,45,46</sup> The potential mechanism for the conversion may be oxidation by hydroxyl radicals on the surfaces of the TiO<sub>2</sub> NMs. In the pH range of 2.0–10.0, Sb(III) exists as Sb(OH)<sub>3</sub>, which can react with the hydroxyl radicals on the surfaces of the TiO<sub>2</sub> NMs, forming a stable surface complex and resulting in the oxidation of Sb(III).<sup>7</sup> It is presumed that the adsorption of Sb(III) on the surfaces of the TiO<sub>2</sub> NMs in aqueous solution involves two processes: direct adsorption and oxidation of Sb(III) to Sb(V). The potential mechanism can be described by eqn (1). Studies on the adsorption of antimony on goethite in the presence of humic acid assumed that the oxidation of trivalent antimony during the adsorption process

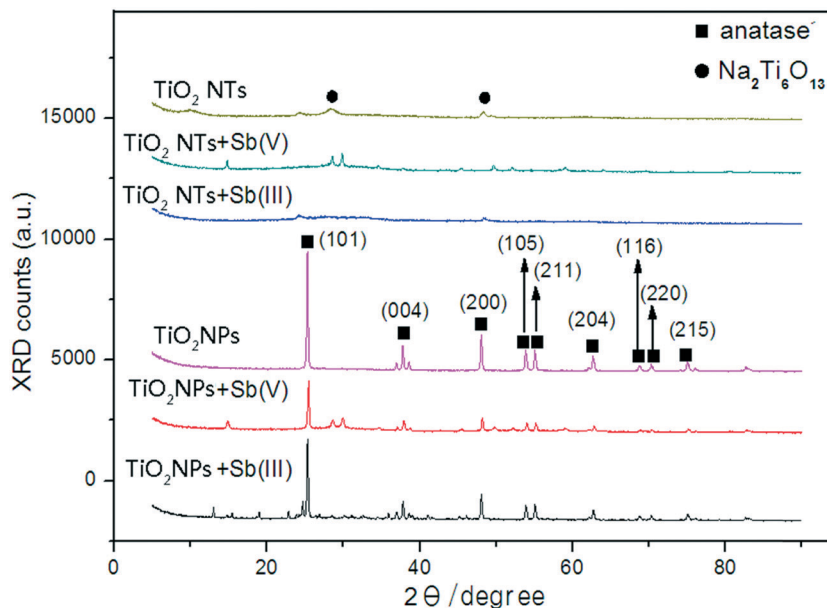


Fig. 3 XRD patterns of  $\text{TiO}_2$  NPs and  $\text{TiO}_2$  NTs before after the adsorption of  $\text{Sb(III)}$  and  $\text{Sb(V)}$ .

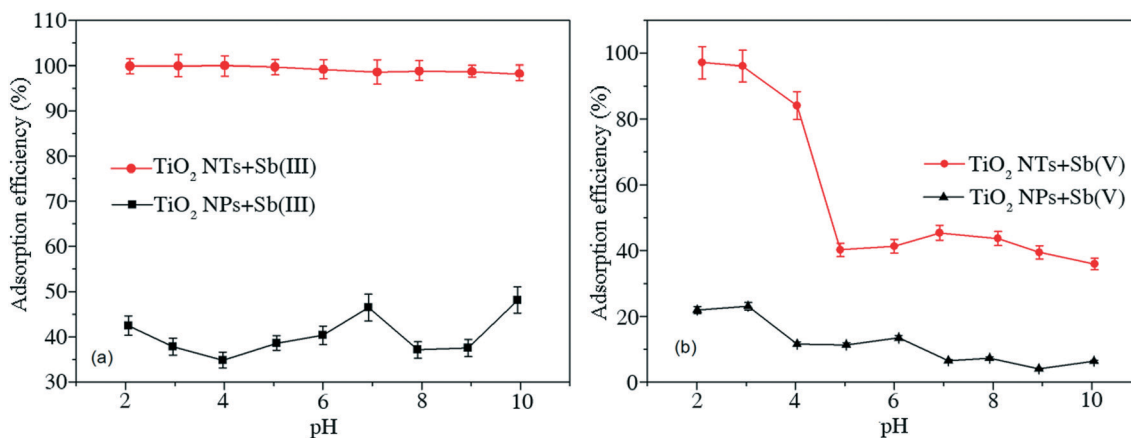
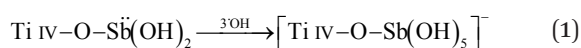


Fig. 4 Effects of pH on  $\text{Sb(III)}$  adsorption on  $\text{TiO}_2$  NPs and  $\text{TiO}_2$  NTs (a) and effect of pH on  $\text{Sb(V)}$  adsorption on  $\text{TiO}_2$  NPs and  $\text{TiO}_2$  NTs (b). Conditions: amount of  $\text{TiO}_2$  NPs and  $\text{TiO}_2$  NTs: 5 mg, concentration of  $\text{Sb(III)}$  and  $\text{Sb(V)}$ :  $1 \text{ mg L}^{-1}$  and solution volume: 50 mL.

results in the formation of a complex with the adsorbent, and then hydroxyl radicals and other groups promote the oxidation of trivalent antimony to pentavalent antimony, which is then released back into solution.<sup>7</sup> However, because a portion of converted  $\text{Sb(V)}$  could also be adsorbed on the surfaces of the  $\text{TiO}_2$  NMs, which could have been removed *via* the filter membrane, its direct quantification is not possible. The concentration of  $\text{Sb(V)}$  on the filters not only depends on the conversion efficiency, but also on the adsorption capacity of the  $\text{TiO}_2$  NMs. Thus, overall, the results suggest that  $\text{TiO}_2$  NTs can accelerate the oxidation of  $\text{Sb(III)}$ , which is beneficial to reduce the toxic potency and environmental risks of  $\text{Sb(III)}$ .



**3.2.2 Adsorption isotherms of  $\text{Sb(III)}$  and  $\text{Sb(V)}$ .** The adsorption isotherms of  $\text{Sb(III)}$  and  $\text{Sb(V)}$  on the  $\text{TiO}_2$  NMs are

shown in Fig. 6. Both the Langmuir (eqn (2)) and Freundlich (eqn (3)) isotherms fit the data well.

$$q_e = \frac{q_m k_L C_e}{1 + k_L C_e} \quad (2)$$

$$q_e = k_F C_e^{1/n} \quad (3)$$

where,  $q_e$  is the amount ( $\text{mg g}^{-1}$ ) of adsorbed  $\text{Sb}$  at equilibrium and  $C_e$  is the equilibrium  $\text{Sb}$  concentration ( $\text{mg L}^{-1}$ ) in solution.  $q_m$  ( $\text{mg g}^{-1}$ ) represents the maximum adsorption amount and  $k_L$  ( $\text{L g}^{-1}$ ) is the Langmuir equilibrium constant. In eqn (3),  $k_F$  ( $\text{mg}^{1-(1/n)} \text{L}^{1/n} \text{g}^{-1}$ ) and  $n$  are the Freundlich parameters.

The related parameters of both models are shown in Table 1. Based on the correlation coefficients, the Langmuir

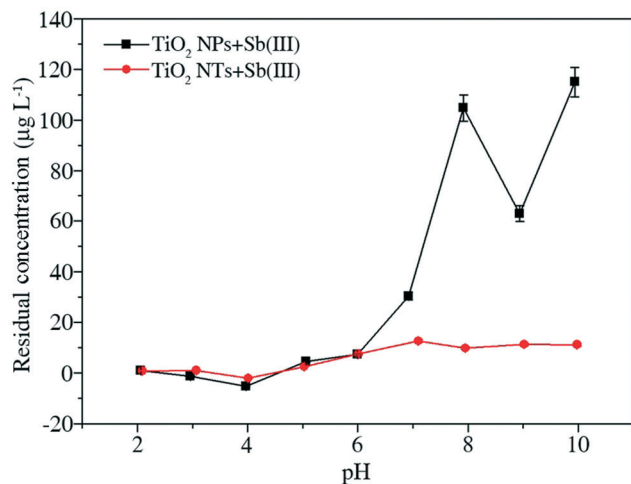


Fig. 5 Residual concentration of Sb(v) converted from Sb(III) after adsorption. Conditions: amount of TiO<sub>2</sub> NPs and TiO<sub>2</sub> NTs: 10 mg, initial concentration of Sb(III): 1 mg L<sup>-1</sup> and solution volume: 50 mL.

isotherm model shows a better fit with the experimental data in comparison to the Freundlich model (Fig. 6) except for Sb(v) adsorbed on the TiO<sub>2</sub> NTs at 15 °C (288.15 K). This result suggests that the adsorption site energy is constant and there is maximum monolayer surface coverage.<sup>22</sup> At 25 °C

(298.15 K), there is a distinct separation between the maximum adsorption amounts of Sb(III) and Sb(v) on the TiO<sub>2</sub> NP and TiO<sub>2</sub> NT surfaces. Specifically, the maximum adsorption amounts were 12.0 mg Sb(III) g<sup>-1</sup> on the TiO<sub>2</sub> NPs, 8.6 mg Sb(v) g<sup>-1</sup> on the TiO<sub>2</sub> NPs, 250.0 mg Sb(III) g<sup>-1</sup> on the TiO<sub>2</sub> NTs and 56.3 mg Sb(v) g<sup>-1</sup> on the TiO<sub>2</sub> NTs. From these results, the adsorption amount of Sb on the TiO<sub>2</sub> NTs was greater than that on the TiO<sub>2</sub> NPs, which was partially due to the BET of the TiO<sub>2</sub> NTs (175.06 m<sup>2</sup> g<sup>-1</sup>), which was 9.2-fold larger than that of the TiO<sub>2</sub> NPs of 19.36 m<sup>2</sup> g<sup>-1</sup>. Furthermore, the maximum adsorption amount of Sb(III) on the TiO<sub>2</sub> NTs was greater than that of other adsorbents, such as carbon nanofibers coated with zirconium oxide,<sup>4</sup> α-FeOOH,<sup>18</sup> Zr-MOFs,<sup>21</sup> α-MnO<sub>2</sub> nanofibers<sup>19</sup> and synthetic manganite (Table S1†).

The Dubinin–Radushkevich (D–R) isotherm model was used to determine the nature of the adsorption process, which fitted the equilibrium data well (Fig. S3 and Table S2†). The mean free energy of Sb(III) and Sb(v) adsorption on the TiO<sub>2</sub> NPs was 8.07 kJ mol<sup>-1</sup> and 8.90 kJ mol<sup>-1</sup> and on the TiO<sub>2</sub> NTs 9.48 kJ mol<sup>-1</sup> and 8.11 kJ mol<sup>-1</sup>, respectively, which indicated that the adsorption of both Sb(III) and Sb(v) is a chemical process in nature.

The increase in adsorption amount with an increase in temperature indicates that the adsorption process is

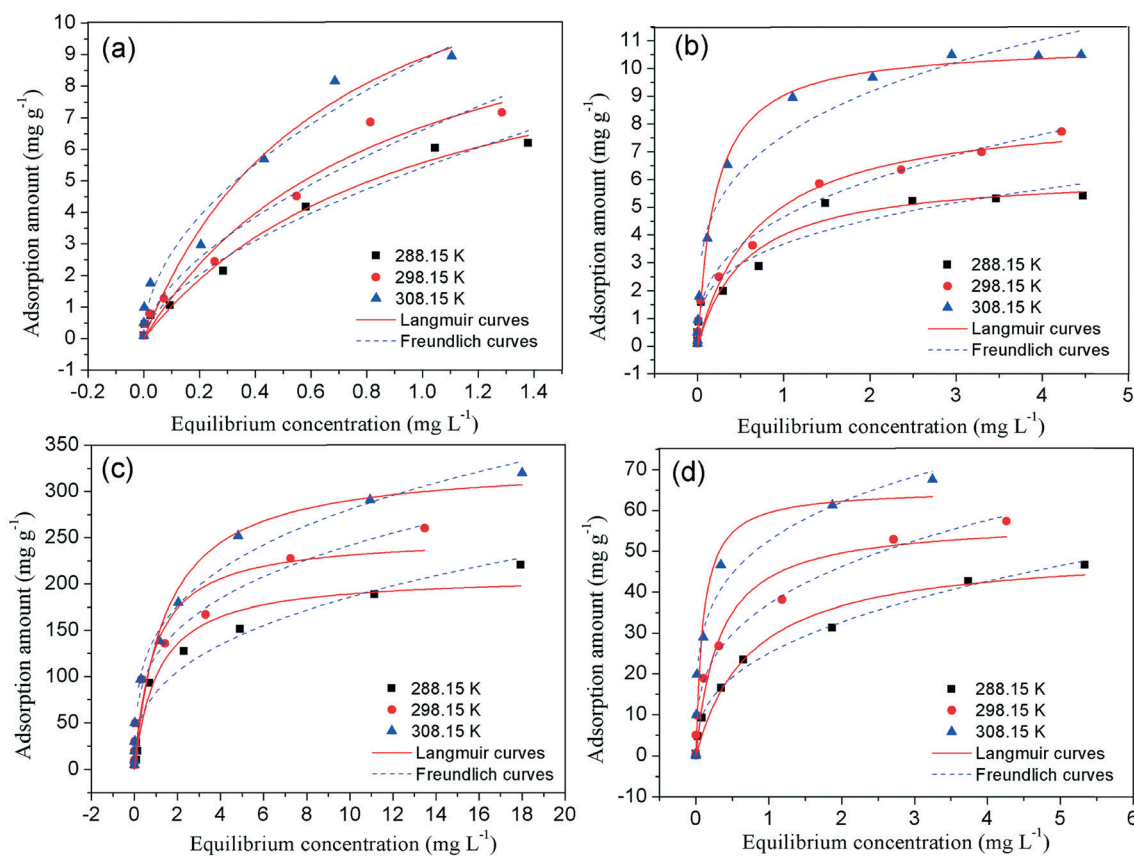


Fig. 6 Adsorption isotherms of Sb(III) adsorbed on TiO<sub>2</sub> NPs (a), Sb(v) on TiO<sub>2</sub> NPs (b), Sb(III) on TiO<sub>2</sub> NTs (c), and Sb(v) on TiO<sub>2</sub> NTs (d). Initial Sb(III) and Sb(v) concentration was 0.01–50 mg L<sup>-1</sup>, adsorbent dose was 5 mg, solution volume was 50 mL and pH was 2.2 ± 0.1.

**Table 1** Langmuir and Freundlich parameters for Sb(III) and Sb(V) adsorption on the TiO<sub>2</sub> NPs and TiO<sub>2</sub> NTs

Langmuir model		Sb(III) + TiO <sub>2</sub> NPs	Sb(V) + TiO <sub>2</sub> NPs	Sb(III) + TiO <sub>2</sub> NTs	Sb(V) + TiO <sub>2</sub> NTs
288.15	$q_m$ (mg g <sup>-1</sup> )	10.9	6.3	209.9	50.5
	$k_L$ (L mg <sup>-1</sup> )	0.97	0.56	1.10	0.756
	$R^2$	0.98	0.97	0.97	0.98
298.15	$q_m$ (mg g <sup>-1</sup> )	12.0	8.6	250.0	56.3
	$k_L$ (L mg <sup>-1</sup> )	0.86	0.70	0.90	0.324
	$R^2$	0.97	0.98	0.98	0.97
308.15	$q_m$ (mg g <sup>-1</sup> )	14.7	10.8	331.6	65.3
	$k_L$ (L mg <sup>-1</sup> )	0.65	0.21	1.42	0.098
	$R^2$	0.98	0.99	0.98	0.98
Freundlich model		Sb(III) + TiO <sub>2</sub> NPs	Sb(V) + TiO <sub>2</sub> NPs	Sb(III) + TiO <sub>2</sub> NTs	Sb(V) + TiO <sub>2</sub> NTs
288.15	$n$	1.64	3.23	2.85	2.61
	$k_F$	5.42	3.67	82.65	25.05
	$R^2$	0.97	0.96	0.95	0.99
298.15	$n$	1.69	2.78	3.39	3.15
	$k_F$	6.61	4.65	122.41	37.08
	$R^2$	0.96	0.98	0.97	0.97
308.15	$n$	1.92	3.70	3.47	4.19
	$k_F$	8.82	7.58	144.55	52.6
	$R^2$	0.96	0.96	0.97	0.98

endothermic. The thermodynamic parameters were also calculated using eqn (4) and (5).

$$\log \left[ \frac{q_e}{C_e} \right] = \frac{\Delta S^0}{2.303R} - \left[ \frac{\Delta H^0}{2.303R} \right] \frac{1}{T} \quad (4)$$

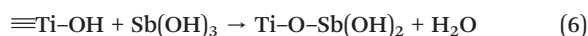
$$\Delta G^0 = \Delta H^0 - T\Delta S^0 \quad (5)$$

where  $\Delta G^0$  is the Gibbs free energy change;  $R$  is the ideal gas constant (8.314 J mol<sup>-1</sup> K<sup>-1</sup>);  $T$  is the absolute temperature (K);  $\Delta H^0$  is the enthalpy change;  $\Delta S^0$  is the entropy change. Based on eqn (4), the  $\Delta H^0$  and  $\Delta S^0$  parameters can be calculated from the slope and intercept of the plot of  $\log(q_e/C_e)$  versus  $1/T$ , respectively (Fig. S4 and Table S3†).

For Sb(III) adsorption on the TiO<sub>2</sub> NTs,  $\Delta H_0$  was calculated to be 3.62 kJ mol<sup>-1</sup>, which indicates that the adsorption process of Sb(III) on the TiO<sub>2</sub> NTs is an endothermic reaction between 15 °C and 35 °C. The  $\Delta S_0$  value of 14.18 J mol<sup>-1</sup> K<sup>-1</sup> is due to the increase in the degrees of freedom of the adsorbed species. The same tendency was observed for the adsorption of Sb(III) and Sb(V) on the TiO<sub>2</sub> NPs and TiO<sub>2</sub> NTs. The desorption thermodynamic properties are important for describing the adsorption properties of sorbents. Thus, desorption experiments were carried out using 0.5 mol L<sup>-1</sup> NaOH as the desorbing agent at 15 °C, 20 °C, 25 °C, 30 °C and 35 °C (Fig. S5†). The desorption efficiency of both Sb(III) and Sb(V) on the TiO<sub>2</sub> NPs and TiO<sub>2</sub> NTs increased with temperature. When the temperature reached 35 °C, the desorption efficiencies of Sb(III) and Sb(V) on the TiO<sub>2</sub> NTs were close to 100% and that on the TiO<sub>2</sub> NPs close to 70%. At the same tempera-

ture, the desorption efficiency of the TiO<sub>2</sub> NTs was significantly greater than that of TiO<sub>2</sub> NPs. Also, the desorption efficiency of Sb(III) was greater than that of Sb(V) on both the TiO<sub>2</sub> NPs and TiO<sub>2</sub> NTs.

The mechanism of adsorption of Sb(V) on the TiO<sub>2</sub> NMs may include electrostatic binding and complexation, and for Sb(III), it is mainly bound by the formation of complexes between Sb(OH)<sub>3</sub> and the hydroxyl functional groups on the surfaces of the TiO<sub>2</sub> NMs (eqn (6) and (7)), as also shown by the FTIR results. Sb(III) is commonly classified as a borderline metal, which can form complexes with ligands containing oxygen- and sulfur-containing groups.<sup>47</sup> Therefore, Sb(III) possibly forms complexes with the hydroxyl functional groups on surfaces of adsorbents, while the adsorption of Sb(V) is the result of electrostatic interactions and complexation.<sup>7,45,48</sup> Previous studies on Sb(V) adsorption on goethite indicated that Sb(V) combines with goethite to form an outer-sphere (FeOH<sub>2</sub><sup>+</sup>-Sb(OH)<sub>6</sub><sup>-</sup>) and an inner-sphere surface complex (Fe-OsB(OH)<sub>6</sub><sup>-</sup>).<sup>7</sup> The  $K_L$  of Sb(III) adsorbed on the TiO<sub>2</sub> NTs was the highest (Table 1), which indicated that the adsorption capacity of the TiO<sub>2</sub> NTs is stronger for Sb(III). This may be due to the fact that the TiO<sub>2</sub> NTs have larger specific surface areas (175.06 m<sup>2</sup> g<sup>-1</sup>) than TiO<sub>2</sub> NPs (19.36 m<sup>2</sup> g<sup>-1</sup>), and thus more adsorption sites. For the formation of inner surface complexes, Sb(V) would occupy more active sites than Sb(III), thus the adsorption amount of Sb(III) is higher than that of Sb(V) on the same adsorbent.<sup>7</sup>



**3.2.3 Adsorption kinetics of Sb(III) and Sb(V).** In practical applications, the rate of adsorption is important when

designing treatments.<sup>4</sup> Adsorption kinetic parameters are critical for designing adsorption units and optimizing operation conditions. The liner plot of the adsorption kinetics is shown in Fig. 7. The kinetics adsorption data was analyzed using the pseudo-first-order (Fig. S6†) and pseudo-second-order models (eqn (8) and (9), respectively).

$$\text{Pseudo-second-order isotherm: } \frac{t}{q_t} = \frac{1}{k_2 q_e^2} + \frac{1}{q_e} t \quad (8)$$

where  $k_2$  is the rate constant of adsorption (in  $\text{g mg}^{-1} \text{min}^{-1}$ ),  $q_t$  is the amount of Sb adsorbed by the adsorbent at any time ( $\text{mg g}^{-1}$ ), and  $q_e$  is the equilibrium adsorption amount ( $\text{mg g}^{-1}$ ). The initial sorption rate  $h_0$  ( $\text{mg g}^{-1} \text{min}^{-1}$ ) can be defined as eqn (9).

$$h_0 = k_2 q_e^2 (t \rightarrow 0) \quad (9)$$

Both  $k_2$  and  $h_0$  were determined experimentally by plotting  $t/q_t$  against  $t$ . All the parameters are listed in Table 2.

The pseudo-second-order kinetic model provides a better correlation with the experimental kinetic data than the pseudo-first-order kinetic model, which indicates that chemical interaction was the rate-controlling step for the adsorption of Sb on the  $\text{TiO}_2$  NMs.<sup>4</sup> The pseudo-second-order kinetic model is based on the assumption that the rate-limiting step may be chemi-

sorption involving exchanging or sharing electrons between the adsorbent and adsorbate.<sup>25,30</sup> The initial rate of adsorption of Sb on the  $\text{TiO}_2$  NTs was significantly greater than that of  $\text{TiO}_2$  NPs, which was partially due to the larger surface areas of the  $\text{TiO}_2$  NTs, providing more active sites for the adsorption of Sb.<sup>36,37</sup> Furthermore, the initial rate of adsorption of Sb(III) on the  $\text{TiO}_2$  NMs was greater than that of Sb(V). This may be due to the fact that the latter occupies more active sites by the formation of complexes during adsorption.

### 3.3 FTIR spectra

The surface chemistry of adsorption was studied using FTIR, which provided information about the mechanisms of adsorption. In the spectra of the  $\text{TiO}_2$  NMs (Fig. 8), the peak at  $489 \text{ cm}^{-1}$  is characteristic of the stretching vibrations of the Ti–O octahedron.<sup>49</sup> Peaks at  $1629 \text{ cm}^{-1}$  and  $3373 \text{ cm}^{-1}$  can be attributed to the stretching vibrations of –COOH or –OH, which indicate the existence of hydroxyl and carboxy groups on the surfaces of the  $\text{TiO}_2$  NTs, respectively. The peak at  $920 \text{ cm}^{-1}$  indicates the presence of Na–O. In the spectra of  $\text{TiO}_2$  NPs/Sb(III) and  $\text{TiO}_2$  NPs/Sb(V), the intensity of the peak at  $3373 \text{ cm}^{-1}$  significantly increased, particularly when Sb(V) was bound to  $\text{TiO}_2$  NPs. A peak at  $1629 \text{ cm}^{-1}$  appeared in the spectra of  $\text{TiO}_2$  NPs/Sb(III) and  $\text{TiO}_2$  NPs/Sb(V), which is ascribed to the stretching vibration of C=O. This peak did not

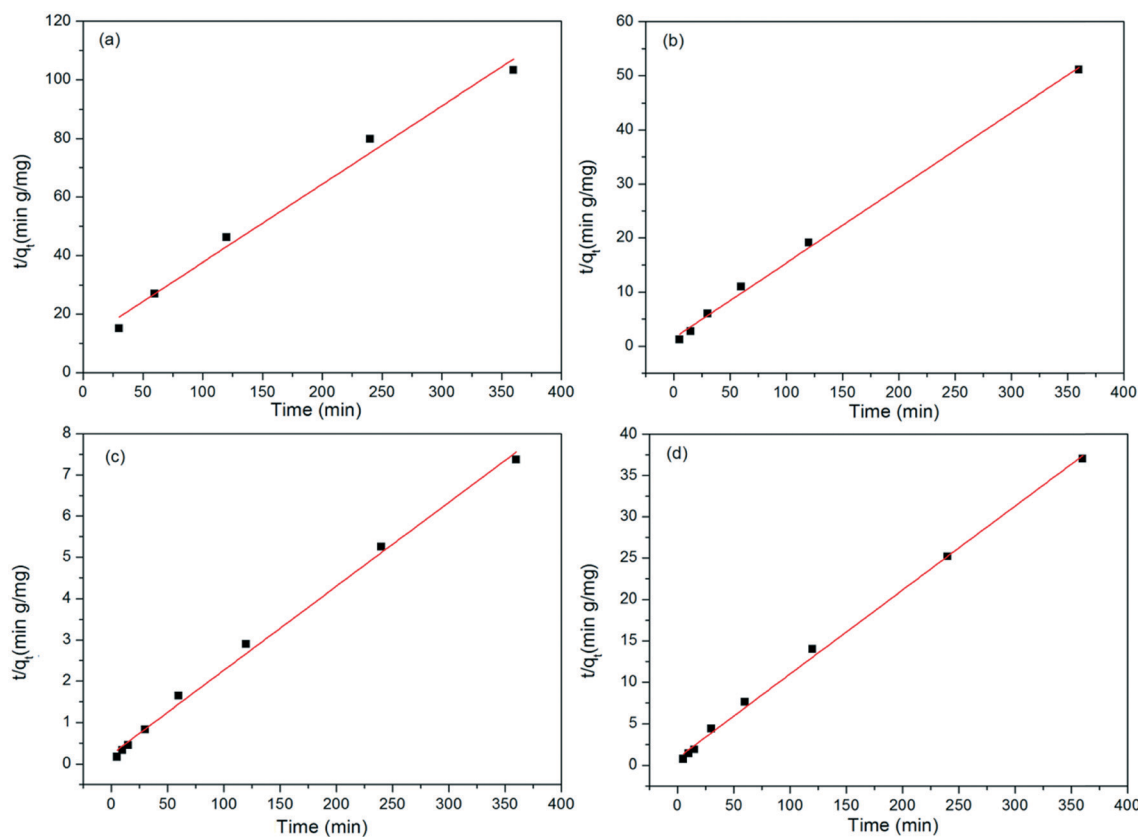


Fig. 7 Pseudo-second-order kinetic curves of Sb(III) adsorbed on  $\text{TiO}_2$  NPs (a), Sb(V) on  $\text{TiO}_2$  NPs (b), Sb(III) on  $\text{TiO}_2$  NTs (c), and Sb(V) on  $\text{TiO}_2$  NTs (d). Initial Sb(III) and Sb(V) concentration was  $10 \mu\text{g L}^{-1}$ – $10 \text{ mg L}^{-1}$ , adsorbent dose was 5 mg, solution volume was 50 mL and pH was  $2.2 \pm 0.1$ .

**Table 2** Pseudo-second-order model kinetic constants for Sb(III) and Sb(V) adsorption on the TiO<sub>2</sub> NPs and TiO<sub>2</sub> NTs

Adsorbent and adsorbate	$k_2$ (g mg <sup>-1</sup> min <sup>-1</sup> )	$h_0$ (mg g <sup>-1</sup> min <sup>-1</sup> )	$q_e$ (mg g <sup>-1</sup> )	$R^2$
Sb(III) on TiO <sub>2</sub> NPs	$1.29 \times 10^{-2}$	0.67	7.19	0.998
Sb(V) on TiO <sub>2</sub> NPs	$0.65 \times 10^{-2}$	0.09	3.75	0.989
Sb(III) on TiO <sub>2</sub> NTs	$0.18 \times 10^{-2}$	4.37	49.02	0.996
Sb(V) on TiO <sub>2</sub> NTs	$1.19 \times 10^{-2}$	1.16	9.85	0.998

appear in the spectrum of TiO<sub>2</sub> NPs. The changes in the peak at 1075 cm<sup>-1</sup> corresponding to the vibration of -OH indicated that -OH combined with Sb.<sup>50</sup> The above results indicate that the successful adsorption of Sb on the surfaces of the TiO<sub>2</sub> NPs occurred through chemical reactions.

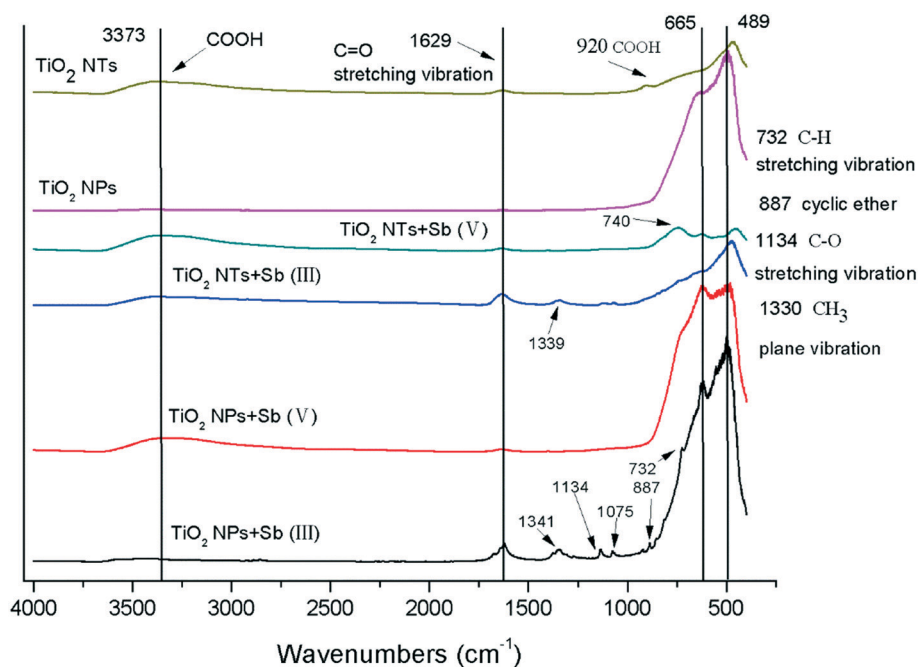
In the spectra of the TiO<sub>2</sub> NTs, TiO<sub>2</sub> NTs/Sb(III) and TiO<sub>2</sub> NTs/Sb(V), there are significant differences in the peak at 1629 cm<sup>-1</sup>, which increased and decreased when Sb(III) and Sb(V) were adsorbed on the TiO<sub>2</sub> NTs, respectively. This may be due to the electrostatic and complexation effects between Sb and the TiO<sub>2</sub> NTs. Sb(III) adsorbed on the surfaces of the TiO<sub>2</sub> NTs also formed complexes. It seems that both hydroxyl and carboxyl groups are involved in the adsorption of both Sb(III) and Sb(V);<sup>51</sup> thus, the intensity of the peak at 1629 cm<sup>-1</sup> significantly increased. The peak at 887 cm<sup>-1</sup> corresponds to the cyclic ether, which also appears in the spectra of the TiO<sub>2</sub> NTs/Sb(III) and TiO<sub>2</sub> NPs/Sb(III) due to the presence of tartaric acid in the solution of the Sb(III) standard used.

### 3.4 XPS

XPS was used to characterize the mechanisms of Sb adsorbed on the TiO<sub>2</sub> NPs and TiO<sub>2</sub> NTs surfaces. The XPS spectra of

TiO<sub>2</sub> NPs, TiO<sub>2</sub> NTs, TiO<sub>2</sub> NPs/Sb(III), TiO<sub>2</sub> NPs/Sb(V), TiO<sub>2</sub> NTs/Sb(III), and TiO<sub>2</sub> NTs/Sb(V) are shown in Fig. 9. The spectrum of the TiO<sub>2</sub> NTs presents a peak at a binding energy of 1070.0 eV for Na, which demonstrates that there were Na atoms on the surfaces of the TiO<sub>2</sub> NTs. This is because the TiO<sub>2</sub> NTs used in this study were synthesized *via* an alkaline hydrothermal method. Although the TiO<sub>2</sub> NTs were pretreated to remove sodium, there was still some residual Na on their surfaces. However, there was no obvious peak for Na in the spectra of TiO<sub>2</sub> NTs/Sb(III) and TiO<sub>2</sub> NTs/Sb(V). There are two possible explanations for, which are Na was replaced by Sb adsorbed on the TiO<sub>2</sub> NTs<sup>52</sup> or crystals of Sb may be around the TiO<sub>2</sub> NTs, and thus Na was not observed in the spectra of TiO<sub>2</sub> NTs/Sb(III) and TiO<sub>2</sub> NTs/Sb(V). Compared to the spectrum of the TiO<sub>2</sub> NPs, a peak for Ti-C appears in the spectrum of TiO<sub>2</sub> NTs, which indicates that C was mixed with the TiO<sub>2</sub> NTs during their formation. There are three peaks in the spectrum of the TiO<sub>2</sub> NMs after Sb was adsorbed. The energetic positions of Pb at 1033.5 eV, Te at 818.7 eV and Mn at 768.0 eV may be due to impurities in the Sb standard.

Survey scans of oxide (O1s) and carbon (C1s) of titanium (Ti) were conducted to identify changes in the states of the elements on the surfaces of the adsorbents. The Ti region did not shift after the adsorption of Sb(III) and Sb(V), but its intensity was significantly lower (Fig. S7<sup>†</sup>), which indicated that Sb(III) and Sb(V) were successfully adsorbed on the surfaces of the TiO<sub>2</sub> NPs and TiO<sub>2</sub> NTs. This binding resulted in crystal-line structures that interfered with the detection of Ti. After Sb(III) and Sb(V) were adsorbed on the surfaces of the TiO<sub>2</sub> NMs, the energetic position and shape of the C1s and O1s peaks were also different (Fig. S8 and S9<sup>†</sup> respectively),

**Fig. 8** FTIR spectra of Sb(III) and Sb(V) adsorbed on TiO<sub>2</sub> NPs and TiO<sub>2</sub> NTs.

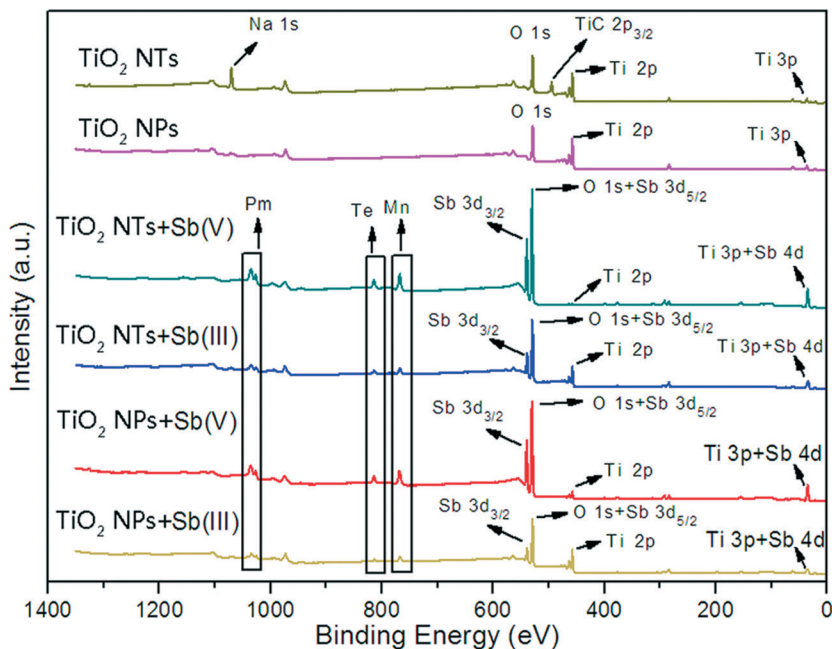


Fig. 9 XPS spectra of TiO<sub>2</sub> NPs, TiO<sub>2</sub> NTs, TiO<sub>2</sub> NPs/Sb(III), TiO<sub>2</sub> NPs/Sb(V), TiO<sub>2</sub> NTs/Sb(III), and TiO<sub>2</sub> NTs/Sb(V).

which indicated that Sb(III) and Sb(V) were successfully adsorbed onto the surfaces of the TiO<sub>2</sub> NPs and TiO<sub>2</sub> NTs, and that the process of adsorption on the TiO<sub>2</sub> NMs was due to chemical binding.

### 3.5 Performance of TiO<sub>2</sub> NPs and TiO<sub>2</sub> NTs in natural water

The adsorption of Sb on the surfaces of TiO<sub>2</sub> NMs in natural water may be more complicated than adsorption in DI water due to the influence of the more complex matrix and various metal ions, organic matter and microbes. Thus, the basic parameters and results of the adsorption on the surfaces of TiO<sub>2</sub> NMs using three types of natural water were examined (Table S4<sup>†</sup>). After 6 h contact with the TiO<sub>2</sub> NPs and TiO<sub>2</sub> NTs, the adsorption amounts of Sb(III) and Sb(V) on the TiO<sub>2</sub> NTs in natural water was higher than that on the TiO<sub>2</sub> NPs, and the adsorption of Sb(III) was higher than Sb(V). The removal efficiency of 200 μg Sb(III) L<sup>-1</sup> by the TiO<sub>2</sub> NTs in the three natural water samples was nearly 100%. Furthermore, the removal efficiency of Sb(V) was inversely proportional to the concentration of TOC and degree of humification. The removal efficiency decreased in the order: tap water (100%) > surface water (99%) > treatment plant effluent (57%). The lower removal efficiencies of Sb in natural water may be due to the effects of anions, such as sulfate and phosphate, in solution, and the presence of dissolved organic matter.<sup>45,60,61</sup> These results demonstrate that the TiO<sub>2</sub> NTs were an effective adsorbent for the removal of trace amounts of Sb not only in DI water, but also in more relevant natural water and wastewater.

The presence of co-existing ions in solution will inevitably impact the adsorption/desorption behavior of adsorbents. Some researchers reported that most univalent and bivalent

ions have no effect on the adsorption of Sb; however, PO<sub>4</sub><sup>3-</sup> can decrease the removal rate of Sb.<sup>15,53–55</sup> This is mainly because PO<sub>4</sub><sup>3-</sup> can also be adsorbed on metal oxides at pH values above the point of zero charge.<sup>56–59</sup> Meanwhile, arsenic (As) also has competitive adsorption with antimony on the surfaces of titanium dioxide, which is attributed to the stronger Lewis base property of Sb(III) than As(III), exhibiting a stronger binding affinity with the Lewis acid Ti5c atoms on the surfaces of TiO<sub>2</sub>.<sup>7</sup> However, the adsorption of Sb(V) was slightly less than As(V) due to the larger octahedral Sb(OH)<sub>6</sub><sup>-</sup> structure than AsO<sub>4</sub><sup>3-</sup>, which has less steric hindrance than the former.<sup>15</sup>

### 3.6 Reusability studies

Reusability was an important factor for an effective adsorbent. Thus, to test the reusability of the TiO<sub>2</sub> NPs and TiO<sub>2</sub> NTs, a desorption study was carried out using NaOH. In our experiments, the adsorbed Sb(III) and Sb(V) were eluted with 0.5 mol L<sup>-1</sup> NaOH since NaOH is known as a very strong chelating agent for many heavy metals. Meanwhile, the surface hydroxyl groups of the TiO<sub>2</sub> NMs became deprotonated and negatively charged at high pH,<sup>36</sup> resulting in efficient desorption of the antimony species, and subsequently Sb(III) and Sb(V) were released into the eluent. The adsorption-desorption cycle was repeated four times using the same sample adsorbent. As the spent adsorbent was recovered, the acquired TiO<sub>2</sub> NPs and TiO<sub>2</sub> NTs were reused for the adsorption of Sb(III) and Sb(V), respectively. The results are shown in Fig. 10, where in contrast with the TiO<sub>2</sub> NPs, the TiO<sub>2</sub> NTs showed excellent reusability. For four consecutive cycles of adsorption-desorption, the removal percentage of TiO<sub>2</sub> NTs to Sb(III) and Sb(V) still reached 85%, and the adsorption

efficiency did not decline significantly. These results demonstrate that the TiO<sub>2</sub> NTs can be used repeatedly without significant loss in their adsorption ability.

### 3.7 DFT calculations

DFT calculations are useful to study the mechanisms of adsorption. In this study, DFT calculations were used to simulate the adsorption of Sb(III) or Sb(V) onto the {101}, {001} and {100} facets of TiO<sub>2</sub> nanoparticles. Based on both empirical results and theoretical calculations, the {101} facet built from anatase-TiO<sub>2</sub> is the most stable.<sup>62,63</sup> The bonding distance between Sb(III) and the TiO<sub>2</sub> substrate was 2.438 Å, which indicated that Sb(III) was successfully adsorbed onto the facet of TiO<sub>2</sub> (Fig. 10a). The pattern of adsorption changed when simulating Sb(III) with two titanium atoms on the {101} facet of TiO<sub>2</sub>. The bond lengths of Sb–O and O–Ti were 3.337 Å and 2.439 Å, respectively (Fig. 10b), which indicated that the Sb(III) tended to be adsorbed on the {101} facet of TiO<sub>2</sub>, which formed ionic bonding between O–Ti atoms. The system energy and bond energy were also calculated to investigate the system stability and preferred adsorption pattern.

For Sb(V) adsorbed onto the TiO<sub>2</sub> {101} facet, the bonding distances of O–Ti (two O atoms of Sb(V) were adsorbed on the same Ti atom) were 2.356 Å and 2.437 Å (Fig. 11c). The H atoms have weak hydrogen bonds with the O atoms in TiO<sub>2</sub> {101} facet as well. Deeper interactions between the O–Ti atoms were also indicated (Fig. 11d). The O–Ti bond length of the Sb(V) molecule adsorbed on three different Ti atoms was 2.129 Å, 2.233 Å and 2.171 Å, respectively, which are shorter than that for the two O atoms of the Sb(V) molecule adsorbed on the same one Ti atom. The Sb(V) atom was located on the top of the Ti atom, which hindered Sb(V) adsorption on the {101} facet of TiO<sub>2</sub> to form a more stable structure (Fig. 11c). The length of the Sb–O bond is 2.671 Å, which formed an ionic bond that is more stable (Fig. 11d). The other two slab models including {001} and {100} simulated by first-principles study based on density functional theory (DFT) are presented in Fig. S10.†

The  $E_{ad}$  value decides the adsorption stability. The adsorption energy ( $E_{ad}$ ) of the Sb molecule was calculated using eqn (10) and shown in Table 3.

$$E_{ad} = E_{\text{surface}} + E_{\text{Sb}} - E_{\text{Sb/surface}} \quad (10)$$

where,  $E_{\text{surface}}$  is the energy of the surface;  $E_{\text{Sb}}$  is the energy of an isolated Sb(III) or Sb(V) molecules;  $E_{\text{Sb/surface}}$  is the total energy of the same molecule adsorbed on the surface. Note that a positive value of  $E_{ad}$  demonstrates stable adsorption.

As shown in Table 3, the adsorption energies ( $E_{ad}$ ) of Sb(III)–1O + one titanium atom (Sb(III), which has one O atom adsorbed onto TiO<sub>2</sub> {101}) and Sb(III)–2O + two titanium atoms (Sb(III), which has two O atoms adsorbed on TiO<sub>2</sub> {101}) onto TiO<sub>2</sub> {101} are equal (1.32 eV). The adsorption energy ( $E_{ad}$ ) of Sb(V)–2O + one titanium atom (Sb(V), which has two O atoms adsorbed onto TiO<sub>2</sub> {101}) (1.72 eV) is higher than that of Sb(V)–3O + three titanium atoms (Sb(V), which has three O atoms adsorbed onto TiO<sub>2</sub> {101}) (1.09 eV) because the three O atoms of Sb(V) tend to form bridges with the Ti atoms in TiO<sub>2</sub> {101}, forming a semi-stable state system. The  $E_{ad}$  of Sb(V) is much higher than that of Sb(III) because Sb(V) is negatively charged and has a larger molecular volume than Sb(III), which hinders the adsorption bonding mode and interactions of the electrons in the 2p orbital of O.

From Table 4, the calculated  $E_{ad}$  of Sb(III) and Sb(V) adsorbed on the {001} facet is 1.13 eV and 3.33 eV, respectively. The adsorbed geometry phase demonstrated that the O atom of Sb(OH)<sub>3</sub> tends to locate on the top position of the Ti atom. For adsorption on the {001} facet, Sb(V) preferred to locate on the plane because Ti bonds with two O atoms to keep equivalent charge density distributions. The  $E_{ad}$  of Sb(III) and Sb(V) adsorbed on the {100} facet is 0.58 eV and 0.07 eV, respectively, which are lower than that for the {101} facet.

Sb(V) prefers to adsorb on the {001} facet to form a more stable structure; however, there is no significant difference between Sb(III) adsorption on the {101} and {001} facets. Stable adsorption structures are derived from the orbital

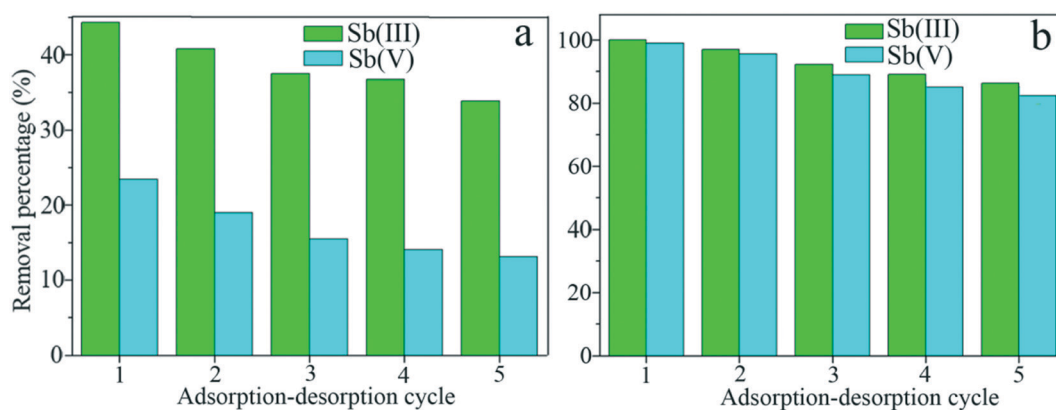
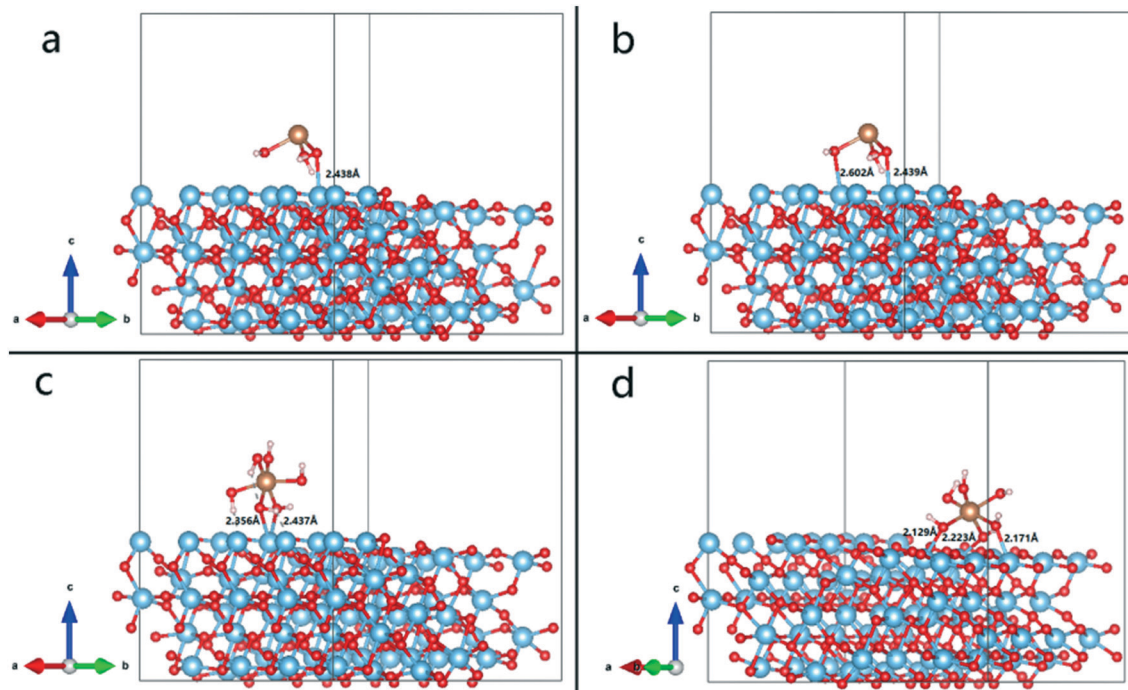


Fig. 10 Adsorption-desorption cycle of TiO<sub>2</sub> NPs (a) and TiO<sub>2</sub> NTs (b). Conditions: amount of TiO<sub>2</sub> NPs and TiO<sub>2</sub> NTs: 5 mg, concentration of Sb(III) and Sb(V): 1 mg L<sup>-1</sup> and solution volume: 50 mL.



**Fig. 11** Optimized  $\text{TiO}_2$  {101} plane slab models for  $\text{Sb(III)}$  adsorption (top). Simulated adsorption of one oxygen atom (a) and two oxygen atoms (b) on  $\text{TiO}_2$  {101}. Antimony atoms are brown, oxygen atoms are red, titanium atoms are light blue, and hydrogen atoms are light pink. Optimized  $\text{TiO}_2$  {101} plane slab model for  $\text{Sb(V)}$  adsorption (bottom). Simulated adsorption of one oxygen atom (c) and three oxygen atoms (d) on  $\text{TiO}_2$  {101}.

**Table 3** Adsorption energy of  $\text{Sb(III)}$  and  $\text{Sb(V)}$  adsorbed on the  $\text{TiO}_2$  {101} facet

	$\text{Sb(III)}-1\text{O} +$ one titanium atom	$\text{Sb(III)}-2\text{O} +$ two titanium atoms	$\text{Sb(V)}-2\text{O} +$ one titanium atom	$\text{Sb(V)}-3\text{O} +$ three titanium atoms
$E_{\text{ad}}$ (eV)	1.23	1.23	1.72	1.09

interactions of each atom, and Sb and Ti are metals, which easily act as donors to bond with O atoms. However, the above observations are inconsistent with that in other studies.<sup>15</sup> This is mainly because the calculation parameters adopted are different in the present study. To eliminate the finite effect in the DFT calculations, which may underestimate the energy upon boundary conditions due to wavefunction overlap, highly accurate parameters were adopted in this study to fix the shortcomings of the formation energy calculations.<sup>64,65</sup> In addition, these calculations provide a clue to distinguish the difference between Sb-based molecules adsorbed on the {001}, {100} and {101} facets.

**Table 4** The adsorption energy ( $E_{\text{ad}}$ ) of  $\text{Sb(III)}$  and  $\text{Sb(V)}$  adsorbed on the  $\text{TiO}_2$  {001}, {100} and {101} facets

	$\text{Sb(III)}$	$\text{Sb(V)}$
{001}	1.13 eV	3.33 eV
{100}	0.58 eV	0.07 eV
{101}	1.23 eV	1.72 eV

## 4. Conclusions

Compared to  $\text{TiO}_2$  nanoparticles, the titanate nanotubes prepared *via* alkaline hydrothermal treatment exhibited greater surface areas and open tube ends, with a lower isoelectric point. The  $\text{TiO}_2$  NTs exhibited fast uptake and significant adsorption capacity for  $\text{Sb(III)}$ , where  $\text{Sb(III)}$  and  $\text{Sb(V)}$  were strongly adsorbed on the surfaces of the  $\text{TiO}_2$  NTs and  $\text{TiO}_2$  NPs and formed crystalline structures that were stable and durable. Solution pH influenced the adsorption of  $\text{Sb(V)}$  on the  $\text{TiO}_2$  NMs. Electrostatic interactions and complexation were predominant in the adsorption of  $\text{Sb(V)}$  and  $\text{Sb(III)}$  on the  $\text{TiO}_2$  NMs, respectively. The  $\text{TiO}_2$  NTs provided abundant active sites due to their large surface areas, which made it possible to adsorb Sb more rapidly.  $\text{Sb(III)}$  may have been converted into  $\text{Sb(V)}$  during adsorption on the surfaces of the  $\text{TiO}_2$  NPs and  $\text{TiO}_2$  NTs, especially at higher pH, and the residual concentration of  $\text{Sb(V)}$  on the  $\text{TiO}_2$  NPs sample was significantly greater than that on the  $\text{TiO}_2$  NTs. In contrast with the  $\text{TiO}_2$  NPs, the  $\text{TiO}_2$  NTs showed excellent reusability with 0.5 mol  $\text{L}^{-1}$  of NaOH solution as the desorbing agent. The FTIR and XPS results indicated that the adsorption of  $\text{Sb(III)}$  and  $\text{Sb(V)}$  had broken the interlayer structure of the  $\text{TiO}_2$  NTs, and both hydroxyl and carboxyl groups were involved in the adsorption. The DFT models suggested that the adsorption originates from complicated crystal structures, which included a six-member ( $\text{Sb(V)}$ ) ring or four-member ( $\text{Sb(III)}$ ) ring on the  $\text{TiO}_2$  {101} facet. The  $\text{TiO}_2$  NTs have superior adsorption performance for Sb species, especially  $\text{Sb(III)}$ , and rate of

their removal is not limited by solution pH. Moreover, in the natural aquatic environment sample, the concentration of Sb was well below the maximum contaminant level for drinking water with a TiO<sub>2</sub> NTs dosage of 0.1 g L<sup>-1</sup>, and titanium dioxide is a safe and non-toxic material, which provides the possibility for the removal of trace Sb in engineering practical treatment of sewage and drinking water.

## Conflicts of interest

There are no conflicts to declare.

## References

- S. Sundar and J. Chakravarty, Antimony toxicity, *Int. J. Environ. Res. Public Health*, 2010, **7**, 4267–4277.
- L. Bregoli, F. Chiarini, A. Gambarelli, G. Sighinolfi, A. M. Gatti, P. Santi, A. M. Martelli and L. Cocco, Toxicity of antimony trioxide nanoparticles on human hematopoietic progenitor cells and comparison to cell lines, *Toxicology*, 2009, **262**, 121–129.
- S. Takahashi, H. Sato, Y. Kubota, H. Utsumi, J. S. Bedford and R. Okayasu, Inhibition of DNA-double strand break repair by antimony compounds, *Toxicology*, 2002, **180**, 249–256.
- J. M. Luo, X. B. Luo, J. Crittenden, J. H. Qu, Y. H. Bai, Y. Peng and J. H. Li, Removal of antimonite (Sb(III)) and antimonate (Sb(V)) from aqueous solution using carbon nanofibers that are decorated with zirconium oxide (ZrO<sub>2</sub>), *Environ. Sci. Technol.*, 2015, **49**, 11115–11124.
- M. C. He, X. Q. Wang, F. C. Wu and Z. Y. Fu, Antimony pollution in China, *Sci. Total Environ.*, 2012, **421–422**, 41–50.
- R. Miravet, J. F. López Sánchez and R. Rubio, New considerations about the separation and quantification of antimony species by ion chromatography-hydride generation atomic fluorescence spectrometry, *J. Chromatogr. A*, 2004, **1052**, 121–129.
- A. K. Leuz, H. Mönch and C. A. Johnson, Sorption of Sb(III) and Sb(V) to goethite: influence on Sb(III) oxidation and mobilization, *Environ. Sci. Technol.*, 2006, **40**, 7277–7282.
- M. Filella, N. Belzile and Y. W. Chen, Antimony in the environment: a review focused on natural waters: I. Occurrence, *Earth-Sci. Rev.*, 2002, **57**, 125–176.
- M. Kang, M. Kawasaki, S. Tamada, T. Kamei and Y. Magara, Effect of pH on the removal of arsenic and antimony using reverse osmosis membranes, *Desalination*, 2000, **131**, 293–298.
- P. Navarro and F. J. Alguacil, Adsorption of antimony and arsenic from a copper electrorefining solution onto activated carbon, *Hydrometallurgy*, 2002, **66**, 101–105.
- Z. J. Wu, M. C. He, X. J. Guo and R. J. Zhou, Removal of antimony (III) and antimony (V) from drinking water by ferric chloride coagulation: Competing ion effect and the mechanism analysis, *Sep. Purif. Technol.*, 2010, **76**, 184–190.
- G. M. Xu, Z. Shi and J. Deng, Characterization of iron oxide coated sand and its adsorption properties in antimony removal, *Huanjing Kexue Xuebao*, 2006, **4017**, 109–121.
- P. P. Song, Z. H. Yang, H. Y. Xu, H. Jing, X. Yang and L. K. Wang, Investigation of influencing factors and mechanism of antimony and arsenic removal by electrocoagulation using Fe–Al electrodes, *Ind. Eng. Chem. Res.*, 2014, **53**, 12911–12919.
- G. S. Zhang, J. H. Qu, H. J. Liu, R. P. Liu and G. T. Li, Removal mechanism of As(III) by a novel Fe–Mn binary oxide adsorbent: oxidation and sorption, *Environ. Sci. Technol.*, 2007, **41**, 4613–4619.
- L. Yan, J. Y. Song, T. S. Chan and C. Y. Jing, Insights into antimony adsorption on {001} TiO<sub>2</sub>: XAFS and DFT Study, *Environ. Sci. Technol.*, 2017, **51**, 6335–6341.
- Y. Q. Leng, W. L. Guo, S. N. Su, C. L. Yi and L. T. Xing, Removal of antimony(III) from aqueous solution by graphene as an adsorbent, *Chem. Eng. J.*, 2012, **211–212**, 406–411.
- X. Q. Zhao, X. M. Dou, D. Mohan, C. U. Pittman Jr, S. O. Yong and X. Jin, Antimonate and antimonite adsorption by a polyvinyl alcohol-stabilized granular adsorbent containing nanoscale zero-valent iron, *Chem. Eng. J.*, 2014, **247**, 250–257.
- X. J. Guo, Z. J. Wu, M. C. He, X. G. Meng, X. Jin, N. Qiu and J. Zhang, Adsorption of antimony onto iron oxyhydroxides: adsorption behavior and surface structure, *J. Hazard. Mater.*, 2014, **276**, 339–345.
- J. M. Luo, C. Z. Hu, X. Y. Meng, J. Crittenden, J. H. Qu and P. Peng, Antimony removal from aqueous solution using novel  $\alpha$ -MnO<sub>2</sub> nanofibers: equilibrium, kinetic, and density functional theory studies, *ACS Sustainable Chem. Eng.*, 2017, **5**, 2255–2264.
- M. A. Salam and R. M. Mohamed, Removal of antimony (III) by multi-walled carbon nanotubes from model solution and environmental samples, *Chem. Eng. Res. Des.*, 2013, **91**, 1352–1360.
- J. Li, X. D. Li, T. Hayat, A. Alsaedi and C. L. Chen, Screening of zirconium-based metal-organic frameworks for efficiently simultaneous removal of antimonite (Sb(III)) and antimonate (Sb(V)) from aqueous solution, *ACS Sustainable Chem. Eng.*, 2017, **5**, 11496–11503.
- J. P. Zou, H. L. Liu, J. M. Luo, Q. J. Xing, H. M. Du, X. H. Jiang, X. B. Luo, S. L. Luo and S. L. L. Suib, Three-dimensional reduced graphene oxide coupled with Mn<sub>3</sub>O<sub>4</sub> for highly efficient removal of Sb(III) and Sb(V) from water, *ACS Appl. Mater. Interfaces*, 2016, **8**, 18140–18149.
- D. W. O'Connell, C. Birkinshaw and T. F. O'Dwyer, Heavy metal adsorbents prepared from the modification of cellulose: A review, *Bioresour. Technol.*, 2008, **99**, 6709–6724.
- K. G. Bhattacharyya and S. S. Gupta, Adsorption of a few heavy metals on natural and modified kaolinite and montmorillonite: A review, *Adv. Colloid Interface Sci.*, 2008, **140**, 114–131.
- S. Haider and S. Y. Park, Preparation of the electrospun chitosan nanofibers and their applications to the adsorption

- of Cu(II) and Pb(II) ions from an aqueous solution, *J. Membr. Sci.*, 2009, **328**, 90–96.
- 26 O. Kasgoz, A. Durmus and A. Kasgoz, Enhanced swelling and adsorption properties of AAm-AMPSNa/clay hydrogel nanocomposites for heavy metal ion removal, *Polym. Adv. Technol.*, 2010, **19**, 213–220.
- 27 T. Wang, W. Liu, N. Xu, L. Xiong and J. R. Ni, Influence of pH, ionic strength and humic acid on competitive adsorption of Pb(II), Cd(II) and Cr(III) onto titanate nanotubes, *Chem. Eng. J.*, 2013, **215**, 366–374.
- 28 X. W. Liu, Q. Y. Hu, Z. Fang, X. I. Zhang and B. B. Zhang, Magnetic chitosan nanocomposites: a useful recyclable tool for heavy metal ion removal, *Langmuir*, 2009, **25**, 3–8.
- 29 X. B. Luo, C. C. Wang, L. C. Wang, F. Deng, S. L. Luo, X. M. Tu and C. T. Au, Nanocomposites of graphene oxide-hydrated zirconium oxide for simultaneous removal of As(III) and As(V) from water, *Chem. Eng. J.*, 2013, **220**, 98–106.
- 30 Y. Tian, M. Wu, R. G. Liu, Y. X. Li, D. Q. Wang, J. J. Tan, R. C. Wu and Y. Huang, Electrospun membrane of cellulose acetate for heavy metal ion adsorption in water treatment, *Carbohydr. Polym.*, 2011, **83**, 743–748.
- 31 P. A. Nishad, A. Bhaskarapillai and S. Velmurugan, Nanotitania-crosslinked chitosan composite as a superior sorbent for antimony (III) and (V), *Carbohydr. Polym.*, 2014, **108**, 169–175.
- 32 B. Mukhopadhyay and S. Lahiri, Adsorption of 125 Sb on alumina and titania surfaces, *J. Radioanal. Nucl. Chem.*, 2007, **273**, 423–426.
- 33 J. F. Banfield and H. Zhang, Nanoparticles in the Environment, *Rev. Mineral. Geochem.*, 2001, **44**, 1–58.
- 34 M. Hua, S. Zhang, B. Pan, W. Zhang, L. Lv and Q. Zhang, Heavy metal removal from water/wastewater by nanosized metal oxides: a review, *J. Hazard. Mater.*, 2012, **211–212**, 317–331.
- 35 W. Liu, P. Zhang, A. G. L. Borthwick, H. Chen and J. R. Ni, Adsorption mechanisms of thallium(I) and thallium(III) by titanate nanotubes: ion-exchange and co-precipitation, *J. Colloid Interface Sci.*, 2014, **423**, 67–75.
- 36 H. Y. Niu, J. M. Wang, Y. L. Shi, Y. Q. Cai and F. S. Wei, Adsorption behavior of arsenic onto protonated titanate nanotubes prepared via hydrothermal method, *Microporous Mesoporous Mater.*, 2009, **122**, 28–35.
- 37 L. Xiong, C. Chen, Q. Chen and J. R. Ni, Adsorption of Pb(II) and Cd(II) from aqueous solutions using titanate nanotubes prepared via hydrothermal method, *J. Hazard. Mater.*, 2011, **189**, 741–748.
- 38 M. Pena, X. Meng, G. P. Korfiatis and C. Jing, Adsorption mechanism of arsenic on nanocrystalline titanium dioxide, *Environ. Sci. Technol.*, 2006, **40**, 1257–1262.
- 39 Q. Chen, W. Z. Zhou, G. H. Du and L. M. Peng, Trititanate nanotubes made via a single alkali treatment, *ChemInform*, 2002, **33**, 219.
- 40 L. Xiong, Y. Yang, J. X. Mai, W. L. Sun, C. Y. Zhang, D. P. Wei, Q. Chen and J. R. Ni, Adsorption behavior of methylene blue onto titanate nanotubes, *Chem. Eng. J.*, 2010, **156**, 313–320.
- 41 M. E. Al-dokheily, Structure and band gap energies of nano titanium dioxide doped with the fifth group elements, *Chem. Process. Eng. Res*, 2014, **25**, 67–75.
- 42 C. K. Lee, K. S. Lin, C. F. Wu, M. D. Lyu and C. C. Lo, Effects of synthesis temperature on the microstructures and basic dyes adsorption of titanate nanotubes, *J. Hazard. Mater.*, 2008, **150**, 494–503.
- 43 F. C. Wu, F. H. Sun, S. Wu, Y. B. Yan and B. S. Xing, Removal of antimony(III) from aqueous solution by freshwater cyanobacteria microcystis biomass, *Chem. Eng. J.*, 2012, **183**, 172–179.
- 44 M. Vithanage, A. U. Rajapaksha, X. M. Dou, N. S. Bolan, J. E. Yang and S. O. Yong, Surface complexation modeling and spectroscopic evidence of antimony adsorption on iron-oxide-rich red earth soils, *J. Colloid Interface Sci.*, 2013, **406**, 217–224.
- 45 J. Buschmann and L. Sigg, Antimony(III) binding to humic substances: influence of pH and type of humic acid, *Environ. Sci. Technol.*, 2004, **38**, 4535–4541.
- 46 N. Belzile, T. W. Chen and Z. Wang, Oxidation of antimony (III) by amorphous iron and manganese oxyhydroxides, *Chem. Geol.*, 2001, **174**, 379–387.
- 47 M. Filella, N. Belzile and Y. W. Chen, Antimony in the environment: A review focused on natural waters II. Relevant solution chemistry, *Earth-Sci. Rev.*, 2002, **59**, 265–285.
- 48 F. H. Sun, F. C. Wu, H. Q. Liao and B. S. Xing, Biosorption of antimony(V) by freshwater cyanobacteria microcystis biomass: Chemical modification and biosorption mechanisms, *Chem. Eng. J.*, 2011, **171**, 1082–1090.
- 49 Y. C. Chen, S. L. Lo and J. Kuo, Pb(II) adsorption capacity and behavior of titanate nanotubes made by microwave hydrothermal method, *Colloids Surf., A*, 2010, **361**, 126–131.
- 50 W. Xu, H. Wang, R. Liu, X. Zhao and J. Qu, The mechanism of antimony(III) removal and its reactions on the surfaces of Fe-Mn binary oxide, *J. Colloid Interface Sci.*, 2011, **363**, 320–326.
- 51 M. Tella and G. S. Pokrovski, Antimony(III) complexing with O-bearing organic ligands in aqueous solution: An X-ray absorption fine structure spectroscopy and solubility study, *Geochim. Cosmochim. Acta*, 2009, **73**, 268–290.
- 52 N. Li, L. Zhang, Y. Chen, Y. Tian and H. Wang, Adsorption behavior of Cu(II) onto titanate nanofibers prepared by alkali treatment, *J. Hazard. Mater.*, 2011, **189**, 265–272.
- 53 M. E. Essington and K. A. Vergeer, Adsorption of antimonate, phosphate, and sulfate by manganese dioxide: competitive effects and surface complexation modeling, *Soil Sci. Soc. Am. J.*, 2015, **79**, 803–804.
- 54 J. H. Xi, M. C. He and C. Y. Lin, Adsorption of antimony(III) and antimony(V) on bentonite: Kinetics, thermodynamics and anion competition, *Microchem. J.*, 2011, **97**, 84–91.
- 55 J. H. Xi, M. C. He and G. Z. Zhang, Antimony adsorption on kaolinite in the presence of competitive anions, *Environ. Earth Sci.*, 2014, **71**, 2989–2997.

- 56 P. A. Connor and A. J. McQuillan, Phosphate adsorption onto  $\text{TiO}_2$  from aqueous solutions: An in situ internal reflection infrared spectroscopic study, *Langmuir*, 1999, **15**, 2916–2921.
- 57 D. Zhao, C. C. Chen, Y. F. Wang, H. W. Ji, W. H. Ma, L. Zang and J. C. Zhao, Surface modification of  $\text{TiO}_2$  by phosphate: Effect on photocatalytic activity and mechanism implication, *J. Phys. Chem. C*, 2008, **112**, 5993–6001.
- 58 J. Antelo, S. Fiol, C. Pérez, S. Mariño, F. Arce, D. Gondar and R. López, Analysis of phosphate adsorption onto ferrihydrite using the CD-MUSIC model, *J. Colloid Interface Sci.*, 2010, **347**, 112–119.
- 59 R. Rahnemaie, T. Hiemstra and W. H. V. Riemsdijk, Geometry, charge distribution, and surface speciation of phosphate on goethite, *Langmuir*, 2007, **23**, 3680–3689.
- 60 B. K. Biswas, J. Inoue, H. Kawakita, K. Ohto and K. Inoue, Effective removal and recovery of antimony using metal-loaded saponified orange waste, *J. Hazard. Mater.*, 2009, **172**, 721–728.
- 61 Z. He, R. Liu, H. Liu and J. Qu, Adsorption of Sb(III) and Sb(V) on freshly prepared ferric hydroxide ( $\text{FeOxHy}$ ), *Environ. Eng. Sci.*, 2015, **32**, 95–102.
- 62 M. Lazzeri, A. Vittadini and A. Selloni, Structure and energetics of stoichiometric  $\text{TiO}_2$  anatase surfaces, *Phys. Rev. B: Condens. Matter Mater. Phys.*, 2001, **63**, 155409.
- 63 F. D. Angelis, G. Vitillaro, L. Kavan, M. K. Nazeeruddin and M. Graetzel, Modeling ruthenium-dye-sensitized  $\text{TiO}_2$  surfaces exposing the (001) or (101) faces: A first-principles investigation, *J. Phys. Chem. C*, 2012, **116**, 18124–18131.
- 64 E. Cho, S. Han, H. S. Ahn, K. R. Lee, S. K. Kim and C. S. Hwang, First-principles study of point defects in rutile  $\text{TiO}_{2-x}$ , *Phys. Rev. B: Condens. Matter Mater. Phys.*, 2006, **73**, 193202.
- 65 B. J. Morgan and G. W. Watson, Intrinsic n-type defect formation in  $\text{TiO}_2$ : a comparison of rutile and anatase from GGA+U calculations, *J. Phys. Chem. C*, 2010, **114**, 2321–2328.

1                                    **Supporting Information (SI)**  
2   **Efficient Removal of Both Antimonite (Sb(III)) and Antimonate**  
3   **(Sb(V)) from Environmental Water Using Titanate nanotubes**  
4   **and nanoparticles**

5

6 Tianhui Zhao,<sup>ab</sup> Zhi Tang,<sup>a</sup> Xiaoli Zhao,<sup>\*a</sup> Hua Zhang,<sup>a</sup> Junyu Wang,<sup>ab</sup> Fengchang Wu,<sup>a</sup>  
7 John P. Giesy,<sup>c</sup> Jia Shi.<sup>d</sup>

8 <sup>a</sup> State Key Laboratory of Environmental Criteria and Risk Assessment, Chinese  
9 Research Academy of Environmental Sciences, Beijing 100012, China.

10 <sup>b</sup> College of Water Sciences, Beijing Normal University, Beijing 100875, China.

11 <sup>c</sup> Department of Veterinary Biomedical Sciences and Toxicology Centre, University  
12 of Saskatchewan, Saskatoon, Saskatchewan, Canada.

13 <sup>d</sup> University of Science and Technology, Beijing, 100083, China

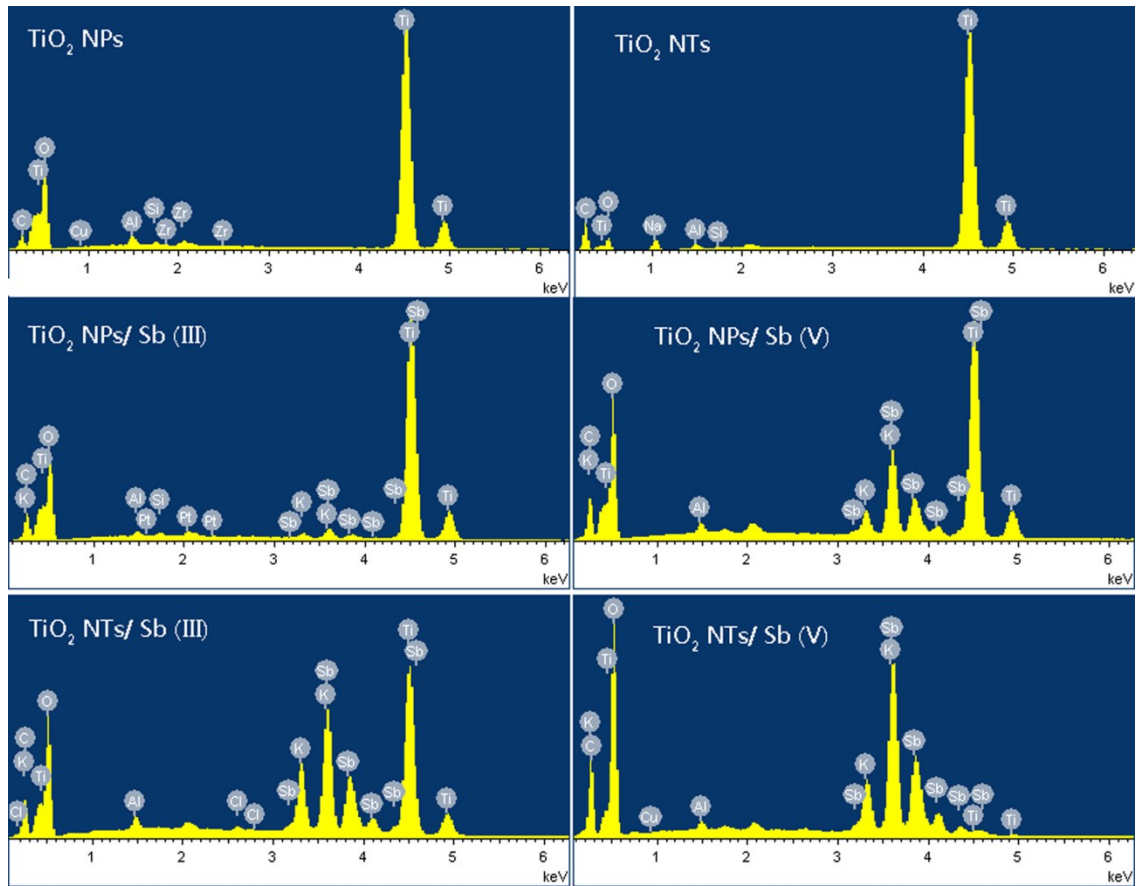
14 Corresponding author.

15 E-mail: [zhaoxiaoli\\_zxl@126.com](mailto:zhaoxiaoli_zxl@126.com)

16

17 Supplemental Information, 19 pages with 10 Figures and 4 Tables

18

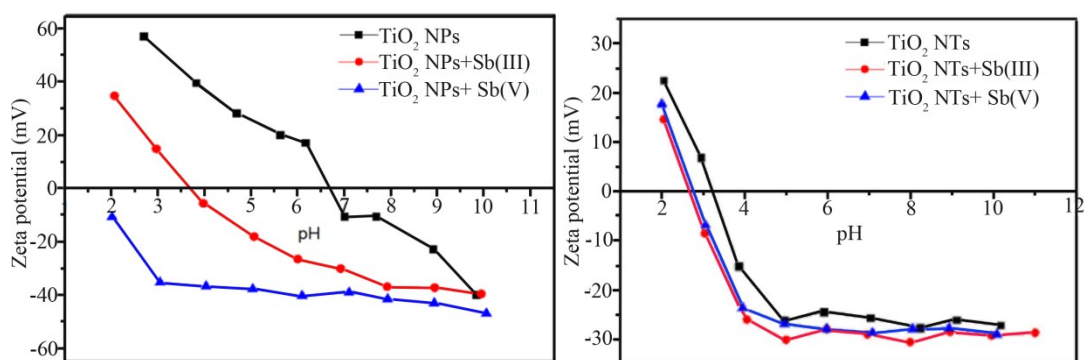


19

20 **Fig.S1 EDX spectras of TiO<sub>2</sub> NPs, TiO<sub>2</sub> NTs, TiO<sub>2</sub> NPs/ Sb (III), TiO<sub>2</sub> NPs/ Sb**  
 21 **(V), TiO<sub>2</sub> NTs/ Sb (III), TiO<sub>2</sub> NTs/ Sb (V)**

22

23 Fig.S2 Changes of Zeta potentials of TiO<sub>2</sub> NPs and TiO<sub>2</sub> NTs before and after  
 24 adsorbing Sb(III) and Sb(V). Adsorption capacity of TiO<sub>2</sub> NTs is greater than that of  
 25 TiO<sub>2</sub> NPs. To compare adsorption of Sb(III) or Sb(V) on surfaces of TiO<sub>2</sub> NPs or TiO<sub>2</sub>  
 26 NTs, changes of Zeta potential of TiO<sub>2</sub> NTs was less than for TiO<sub>2</sub> NPs. Electrostatic  
 27 interactions are the primary mechanism of adsorption of Sb(V) on TiO<sub>2</sub> NMs.  
 28 Positive charges on surfaces of TiO<sub>2</sub> NMs were neutralized by compounds of Sb(V).  
 29 Meanwhile, complexation played a dominant role in adsorption of Sb (III) on TiO<sub>2</sub>  
 30 NMs. Changes of Zeta potential of Sb(V) adsorbed onto TiO<sub>2</sub> NMs may be due to  
 31 forming a stable inner complex.<sup>14,15</sup>



32  
 33 **Fig.S2 Zeta potentials of adsorption of Sb(III) and Sb(V) on TiO<sub>2</sub> NPs and TiO<sub>2</sub>**  
 34 **NTs**  
 35

36 The Dubinin–Radushkevich (D-R) isotherm model can be used to determine the  
37 nature of the adsorption process (physical or chemical).<sup>11</sup> The linear equation of the  
38 D-R isotherm is expressed as Equation 1 and 2:<sup>15</sup>

$$39 \quad \ln Q_e = \ln Q_{DR} - \beta \varepsilon^2 \quad (1)$$

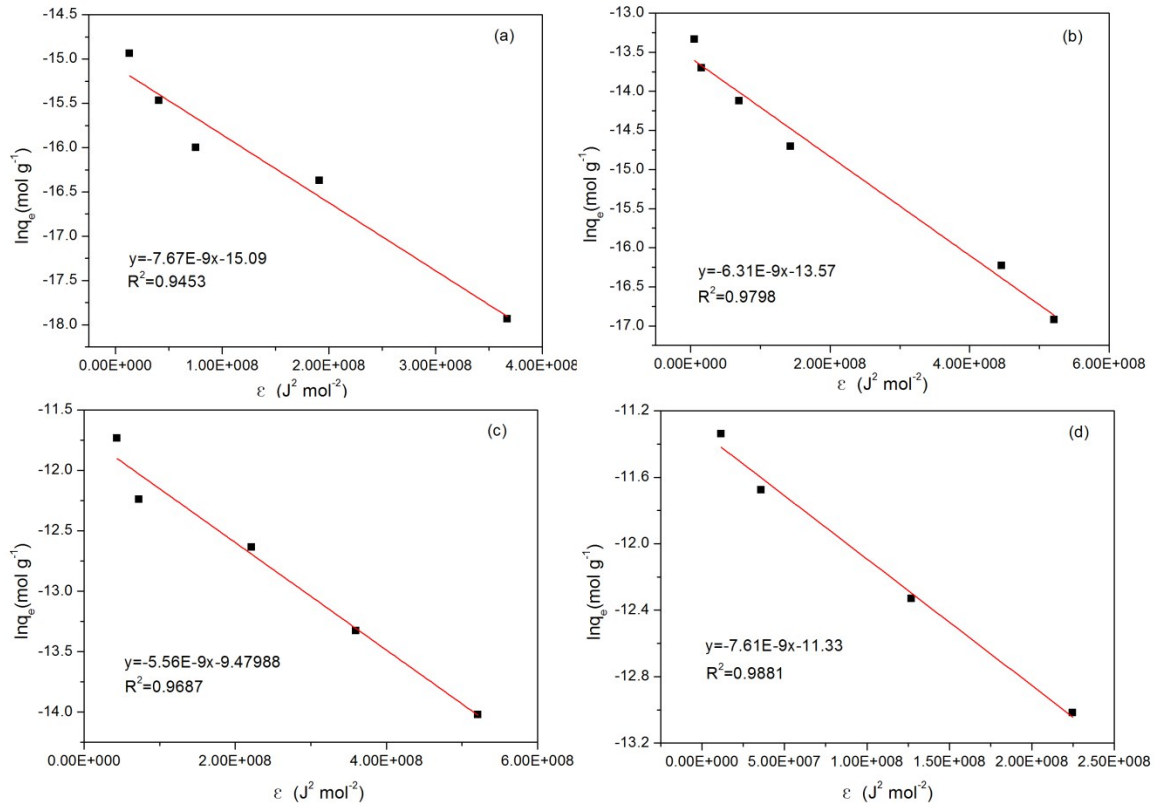
$$40 \quad \varepsilon = RT \ln \left( 1 + 1/C_e \right) \quad (2)$$

41 where  $q_e$  is the amount of metal ions sorbed per unit weight of adsorbent (mol  
42 L<sup>-1</sup>),  $q_m$  is the maximum adsorption capacity (mol g<sup>-1</sup>),  $\beta$  is the activity coefficient  
43 related to the mean free energy of adsorption (mol<sup>2</sup> J<sup>-2</sup>),  $R$  is the gas constant (8.314 J  
44 (mol K)<sup>-1</sup>);  $T$  is the thermodynamic temperature (K); and  $\varepsilon$  is the Polanyi potential.

45 The D-R isotherm model fits the equilibrium data well (Figure S3 and Table S2),  
46  $R^2$  values were 0.95, 0.98, 0.97, 0.99 for Sb(III) and Sb(V) adsorption on TiO<sub>2</sub> NPs  
47 and TiO<sub>2</sub> NTs, respectively. The mean free energy of adsorption ( $E$ ; kJ (J mol)<sup>-1</sup>) is  
48 expressed as Equation 3:

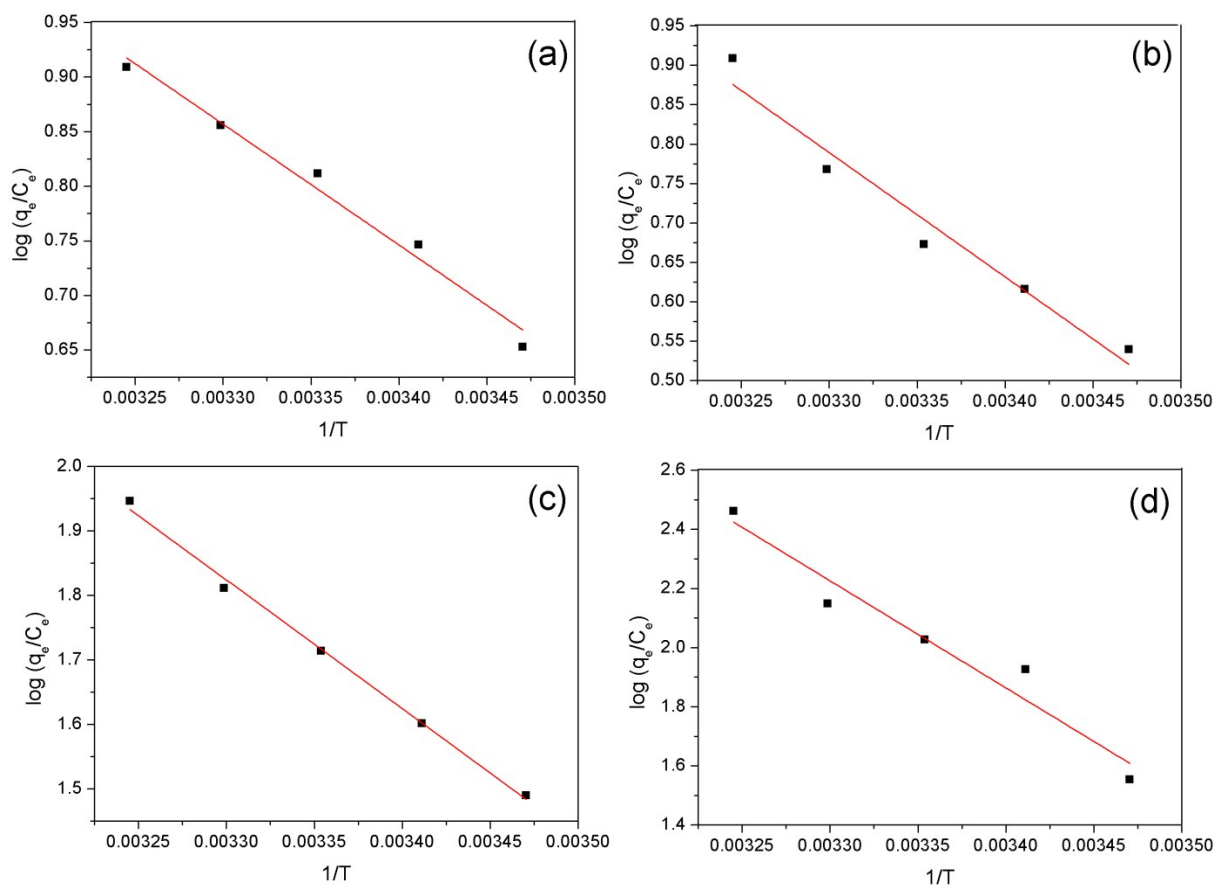
$$49 \quad E = \frac{1}{\sqrt{2\beta}} \quad (3)$$

50 The adsorption behavior might be predicted, whether physical or chemical  
51 process, from the  $E$  value, which in the range of 8-16 kJ mol<sup>-1</sup> is ion-exchange  
52 reaction. The mean free energy of Sb(III) and Sb(V) adsorption on TiO<sub>2</sub> NPs were  
53 8.07, 8.90 kJ mol<sup>-1</sup> and on TiO<sub>2</sub> NTs were 9.48 and 8.11 kJ mol<sup>-1</sup>, respectively, which  
54 indicated the both Sb(III) and Sb(V) adsorption are chemical process in nature.



55

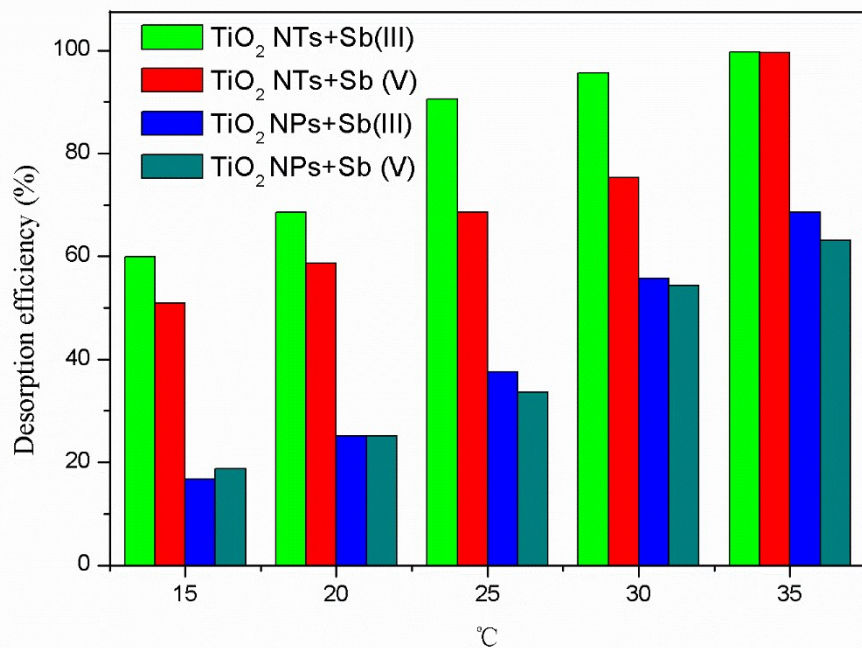
56 **Fig.S3 Dubinin–Radushkevich (D-R) isotherm models of Sb(III) adsorbed on**  
 57 **TiO<sub>2</sub> NPs (a), Sb(V) on TiO<sub>2</sub> NPs (b), Sb(III) on TiO<sub>2</sub> NTs (c), Sb(V) on TiO<sub>2</sub> NTs**  
 58 **(d). adsorbent dose was 5 mg; the solution volume was 50 mL; pH was 2.2 ± 0.1**



60

61 **Fig.S4 Adsorption thermodynamics of Sb(III) adsorbed on TiO<sub>2</sub> NPs (a), Sb(V)**  
 62 **on TiO<sub>2</sub> NPs (b), Sb(III) on TiO<sub>2</sub> NTs (c), Sb(V) on TiO<sub>2</sub> NTs (d). adsorbent dose**  
 63 **was 5 mg; the solution volume was 50 mL; pH was  $2.2 \pm 0.1$ ; The temperature**  
 64 **was 15, 20, 25, 30, 35 °C**

65

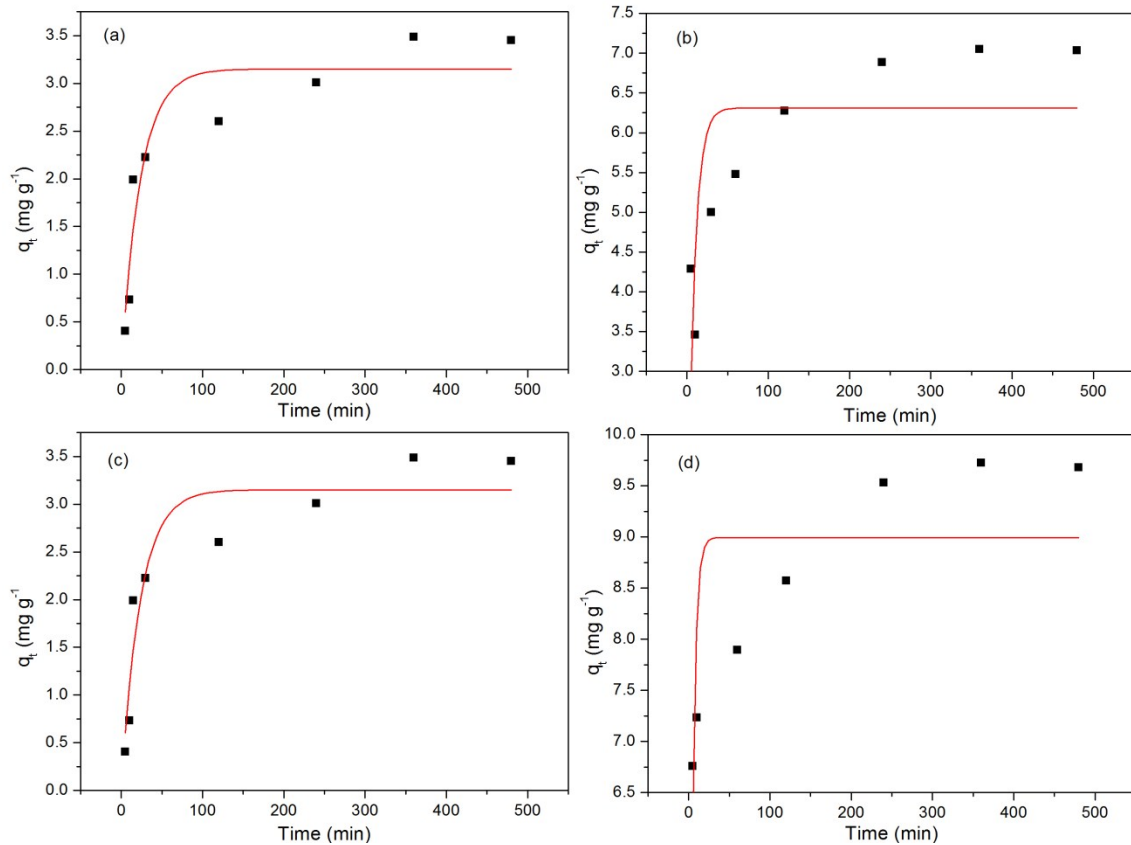


66

67 **Fig.S5 Desorption thermodynamics of Sb(III) adsorbed on TiO<sub>2</sub> NPs, Sb(V) on**  
 68 **TiO<sub>2</sub> NPs, Sb(III) on TiO<sub>2</sub> NTs, Sb(V) on TiO<sub>2</sub> NTs. adsorbent dose was 5 mg;**  
 69 **the solution volume was 50 mL; desorbing agent was 0.1 mol L<sup>-1</sup> NaOH; The**

70 **temperature was 15, 20, 25, 30, 35 °C**

71



72

73 **Fig.S6 Pseudo-first-order kinetic curves of Sb(III) adsorbed on TiO<sub>2</sub> NPs (a),**  
 74 **Sb(V) on TiO<sub>2</sub> NPs (b) , Sb(III) on TiO<sub>2</sub> NTs (c), Sb(V) on TiO<sub>2</sub> NTs (d). Initial**  
 75 **Sb(III) and Sb(V) concentration was 10 μg L<sup>-1</sup> - 10 mg L<sup>-1</sup>; adsorbent dose was 5**  
 76 **mg; the solution volume was 50 mL; and pH was 2.2 ± 0.1**

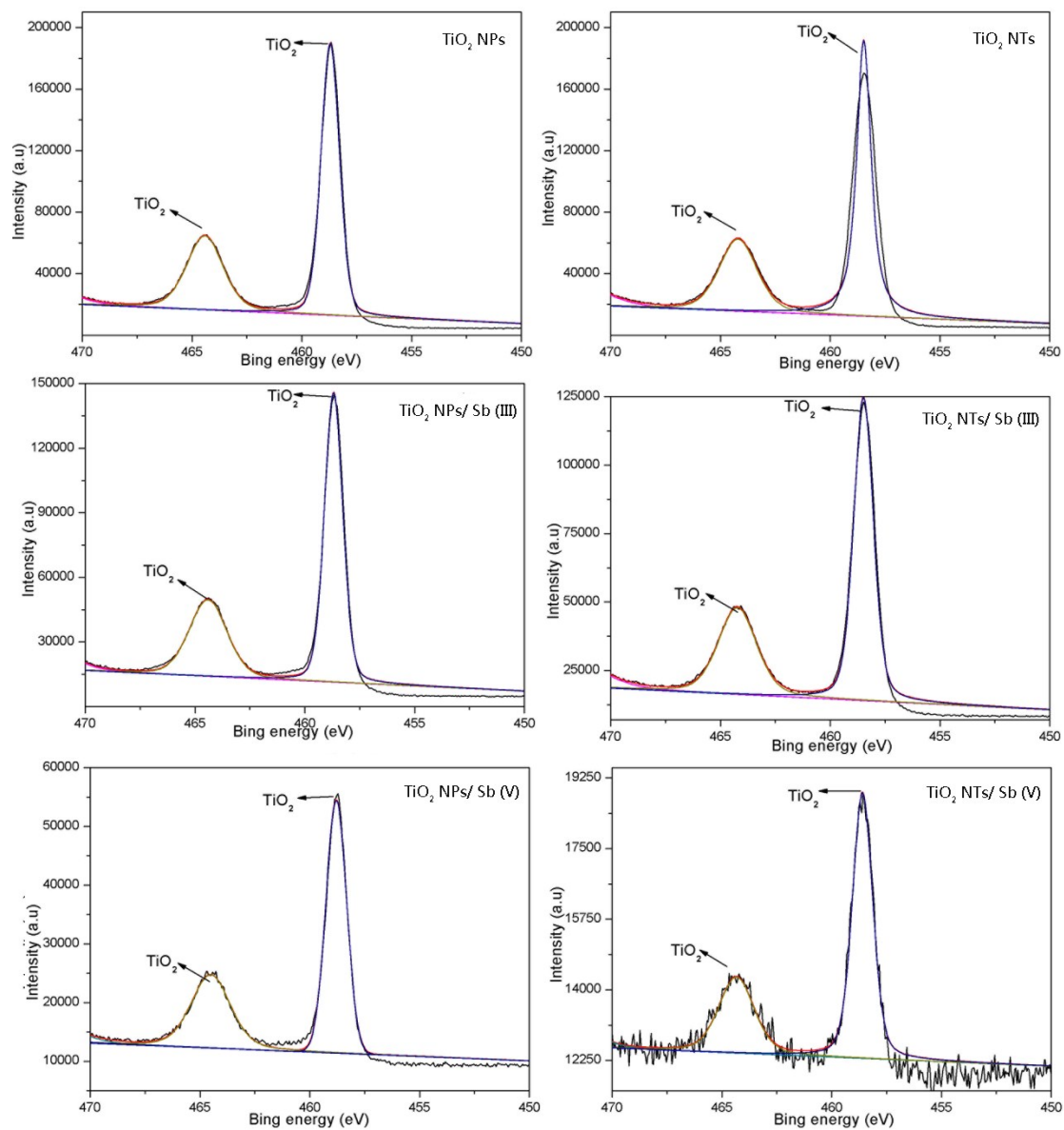
77

78 Pseudo-first-order kinetic models are expressed as Equation 4:

$$79 \quad q_t = q_e(1 - e^{-k_1 t}) \quad (4)$$

80 Where  $q_e$  is the amount of adsorbate at equilibrium (mg g<sup>-1</sup>);  $q_t$  is the amount of  
 81 adsorbate (mg g<sup>-1</sup>) at time  $t$  (min); and  $K_1$  (min<sup>-1</sup>) and  $K_2$  (g mg·min<sup>-1</sup>) are the rate  
 82 constants for the pseudo first-order sorption, respectively.

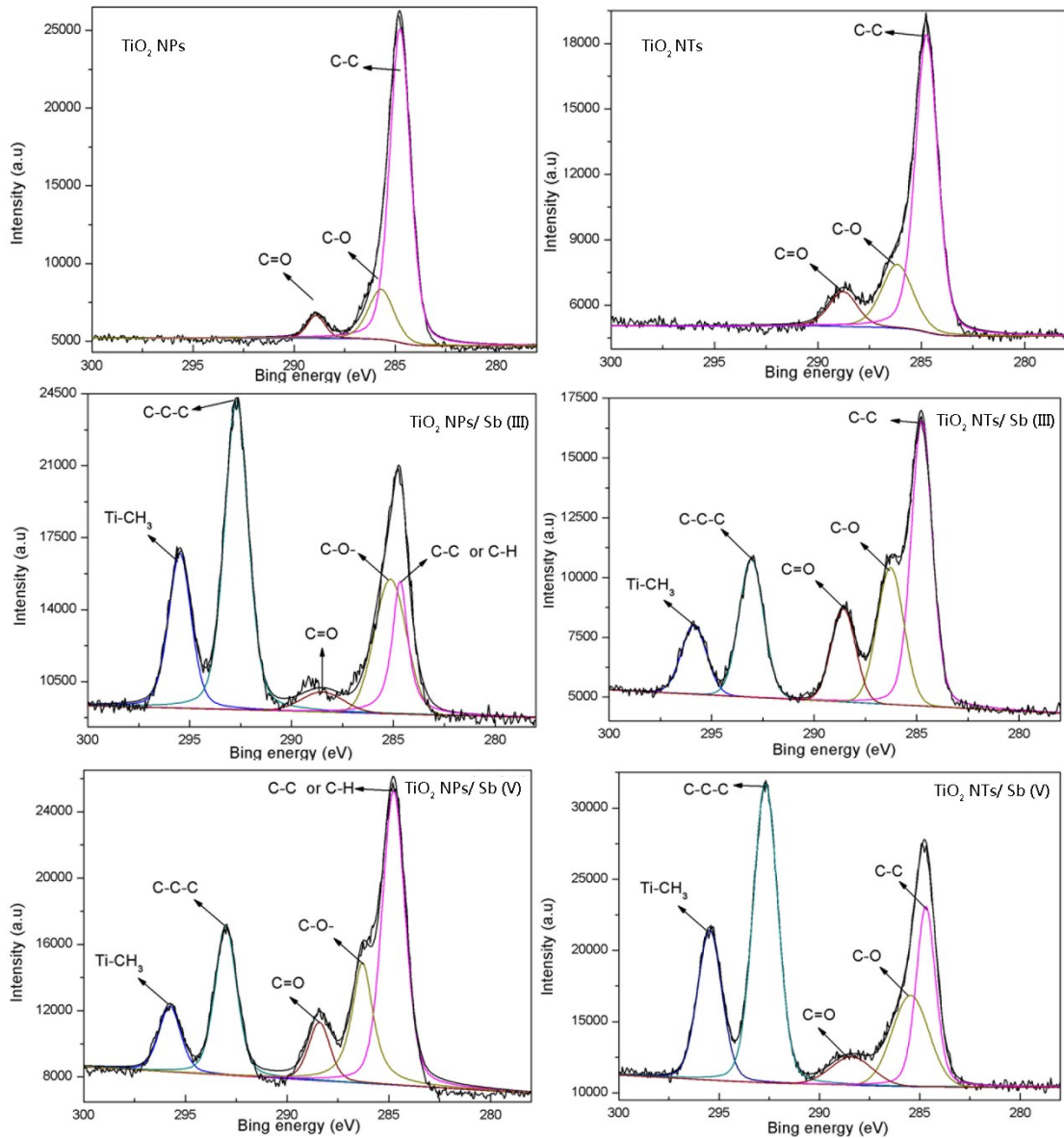
83



85

86 Fig.S7 XPS spectras of Ti for TiO<sub>2</sub> NPs, TiO<sub>2</sub> NTs, TiO<sub>2</sub> NPs/ Sb (III), TiO<sub>2</sub> NPs/  
 87 Sb (V), TiO<sub>2</sub> NTs/ Sb (III), TiO<sub>2</sub> NTs/ Sb (V)

88



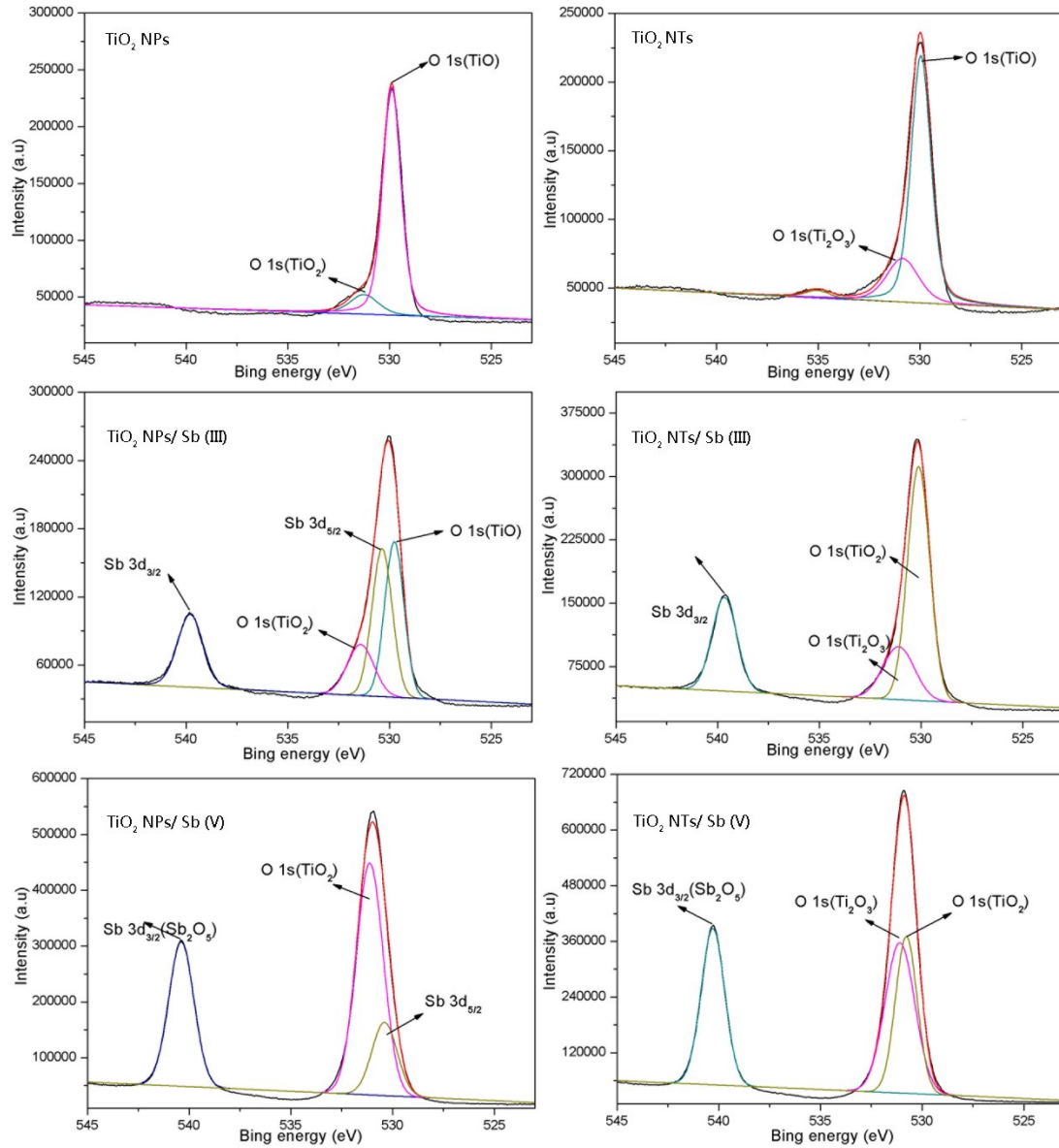
89

90 **Fig.S8 XPS spectra of C1s for TiO<sub>2</sub> NPs, TiO<sub>2</sub> NTs, TiO<sub>2</sub> NPs/ Sb (III), TiO<sub>2</sub>**  
 91 **NPs/ Sb (V), TiO<sub>2</sub> NTs/ Sb (III), TiO<sub>2</sub> NTs/ Sb (V)**

92

93

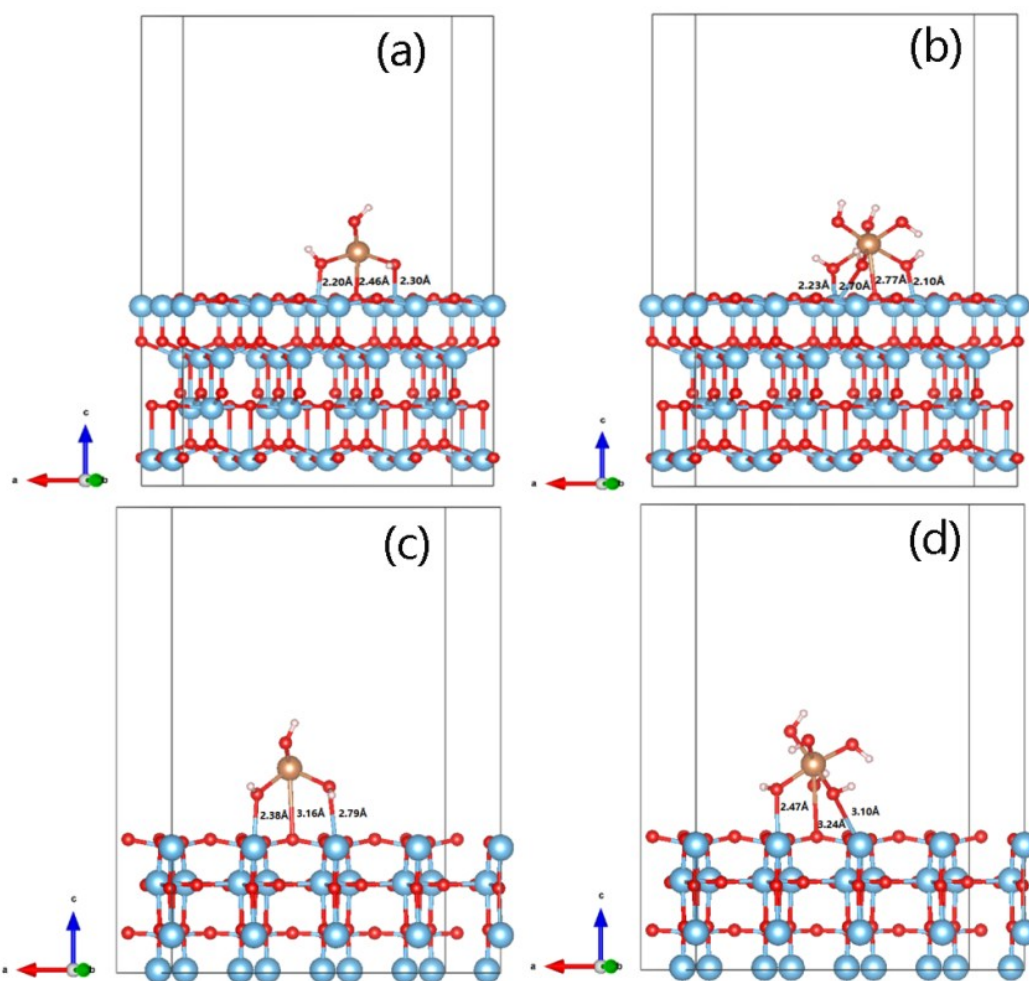
94



95

96 **Fig.S9 XPS spectras of O1s for TiO<sub>2</sub> NPs, TiO<sub>2</sub> NTs, TiO<sub>2</sub> NPs/ Sb (III), TiO<sub>2</sub>**  
 97 **NPs/ Sb (V), TiO<sub>2</sub> NTs/ Sb (III), TiO<sub>2</sub> NTs/ Sb (V)**

98



99

100 **Fig.S10 Optimized  $\text{TiO}_2$  {001} plane slab models for Sb(III) adsorption (a) and**  
 101 **Sb(V) adsorption (b), optimized  $\text{TiO}_2$  {100} plane slab models for Sb(III)**  
 102 **adsorption (c) and Sb(V) adsorption (d)**

103

104 As shown in Figure. 10a, two O atoms of Sb(III) bond with two Ti atoms. The  
 105 bond length of Ti-O is 2.20 and 2.30 Å, respectively. As shown in Figure. 10b, three  
 106 O atoms of Sb(V) bond with two Ti atoms, the Ti-O length is 2.10 Å, 2.23 Å and 2.70  
 107 Å, respectively.

108 Comparing to adsorption results of {001} facet, Sb(III) and Sb(V) adsorbed on  
 109 {100} facet is slightly loose. As shown in Figure 10c and 10d, the adsorption pattern  
 110 of Sb(III) adsorbed on {100} facet is same with the {001} facet. The Ti-O bond  
 111 length is 2.38 Å and 2.79 Å. The two O atoms of Sb(V) adsorbed on Ti atoms  
 112 respectively, Ti-O bond length is 2.47 Å and 3.10 Å.

113

**Table S1 Comparison of performance of TiO<sub>2</sub> NTs (present study) and various adsorbents for removal of Sb from water.**

114

Adsorbents	Concentration range (initial concentration mg L <sup>-1</sup> )	pH	Dose (g L <sup>-1</sup> )	Adsorption amount (mg g <sup>-1</sup> )		References
				Sb (III)	Sb (V)	
TiO <sub>2</sub> NTs(Present study)	0.01-10	2.0-10.0	0.1	250.00	56.30	-
carbon nanofibers decorated with zirconium oxide (ZrO <sub>2</sub> )	10-500	7.0 ± 0.2	1.0	70.83	57.17	1
Activated alumina	5-75	2.0-11.0	1.0	-	38.00	2
Nanoscale zero-valent iron	0-20	4.0-10.0	2.0	6.99	1.65	3
Hematite coated magnetic nanoparticle	1-20	4.1	0.1	36.70	-	4
Synthetic manganite	0.5-98	3.0	0.6	-	95.00	5
Iron-zirconium bimetal oxide	0-25	7.0	0.2	-	51.00	6
α-FeOOH	-	2.0-12.0	25.0	-	48.70	7
Kaolinite	1	6.0	25.0	-	12.00	8
Diatomite	10-400	6.0	4.0	35.20	-	9

Cyanobacteria	10	2.0–7.0	0.8-20.0	4.88	-	10
Zr-MOFs	2-500	2.3-9.5	0.8	136.97	287.88	11
$\alpha$ -MnO <sub>2</sub> Nanofibers	10-500	4.0	0.5	111.70	89.99	12
Reduced graphene oxides/Mn <sub>3</sub> O <sub>4</sub>	10–1000	2.5–11.5	1.0	151.84	105.50	13

116

**Table S2 D-R isotherm parameters for Sb(III) and Sb(V) adsorption on TiO<sub>2</sub> NPs and TiO<sub>2</sub> NTs.**

Adsorbed types	D-R isotherm model		
	$q_m$ ' (mol g <sup>-1</sup> )	$\beta$ (mol <sup>2</sup> J <sup>-2</sup> )	R <sup>2</sup>
Sb(III)+ TiO <sub>2</sub> NPs	$1.24 \times 10^{-7}$	$7.67 \times 10^{-9}$	0.95
Sb(V)+ TiO <sub>2</sub> NPs	$1.28 \times 10^{-6}$	$6.31 \times 10^{-9}$	0.98
Sb(III)+ TiO <sub>2</sub> NTs	$7.64 \times 10^{-5}$	$5.56 \times 10^{-9}$	0.97
Sb(V)+ TiO <sub>2</sub> NTs	$1.20 \times 10^{-5}$	$7.61 \times 10^{-9}$	0.99

117

118

**Table S3 Thermodynamics of adsorption of Sb(III) and Sb(V) on TiO<sub>2</sub> NPs and TiO<sub>2</sub> NTs**

Adsorbed types	$\Delta H^0$ (KJ mol <sup>-1</sup> )	$\Delta S^0$ (J mol <sup>-1</sup> K <sup>-1</sup> )	$-\Delta G^0$ (KJ mol <sup>-1</sup> )				
			15°C	20°C	25°C	30°C	35°C
Sb(III)+TiO <sub>2</sub> NPs	1.11	4.51	0.19	0.21	0.23	0.26	0.28
Sb(V)+TiO <sub>2</sub> NPs	1.58	5.98	0.14	0.17	0.20	0.23	0.26
Sb(V)+TiO <sub>2</sub> NTs	3.62	14.18	0.47	0.54	0.61	0.68	0.75
Sb(III)+TiO <sub>2</sub> NTs	1.99	8.40	0.43	0.47	0.51	0.56	0.60

119

120

**Table S4 Efficiencies of removal of Sb by TiO<sub>2</sub> NMs in natural water**

Real water	TOC mg L <sup>-1</sup>	UV 465/665	TiO <sub>2</sub> NPs/Sb(III)		TiO <sub>2</sub> NPs/Sb(V)		TiO <sub>2</sub> NTs/Sb(III)		TiO <sub>2</sub> NTs/Sb(V)	
			Adsorbed amount (mg g <sup>-1</sup> )	Removal efficiency (%)						
Tap water	3.62	0.032	104.63	52	89.44	44	199.88	100	199.58	100
Landscape water	10.83	0.076	68.64	34	30.49	15	199.64	100	198.13	99
Treatment plant effluent	20.85	0.228	82.93	41	47.80	23	199.82	100	113.66	57

121

122 **References**

- 123 1 J.M. Luo, X.B. Luo, J. Crittenden, J.H. Qu, Y.H. Bai, Y. Peng and J.H. Li, Removal  
124 of antimonite (Sb(III)) and antimonate (Sb(V)) from aqueous solution using carbon  
125 nanofibers that are decorated with zirconium oxide (ZrO<sub>2</sub>), *Environ. Sci. Technol.*,  
126 2015, **49**, 11115-11124.
- 127 2 Y.H. Xu, A. Ohki and S. Maeda, Adsorption and removal of antimony from  
128 aqueous solution by an activated alumina, *Toxicol. Environ. Chem.*, 2001, **80**, 145-  
129 154.
- 130 3 X.Q. Zhao, X.M. Dou, D. Mohan, C.U. Pittman Jr, S.O. Yong and X. Jin,  
131 Antimonate and antimonite adsorption by a polyvinyl alcohol-stabilized granular  
132 adsorbent containing nanoscale zero-valent iron, *Chem. Eng. J.*, 2014, **247**, 250-257.
- 133 4 C. Shan, Z.Y. Ma and M.P. Tong, Efficient removal of trace antimony(III) through  
134 adsorption by hematite modified magnetic nanoparticles, *J. Hazard. Mater.*, 2014,  
135 **268**, 229-236.
- 136 5 X.Q. Wang, M.C. He, C.Y. Lin, Y.X. Gao and L. Zheng, Antimony(III) oxidation  
137 and antimony(V) adsorption reactions on synthetic manganite, *Chem. Erde.*  
138 *Geochem.*, 2012, **72**, 41-47.
- 139 6 X.H. Li, X.M. Dou and J.Q. Li, Antimony(V) removal from water by iron -  
140 zirconium bimetal oxide: performance and mechanism, *J. Environ. Sci.*, 2012, **24**,  
141 1197-1203.
- 142 7 X.J. Guo, Z.J. Wu, M.C. He, X.G. Meng, X. Jin, N. Qiu and J. Zhang, Adsorption  
143 of antimony onto iron oxyhydroxides: adsorption behavior and surface structure, *J.*  
144 *Hazard. Mater.*, 2014, **276**, 339-345.
- 145 8 J.H. Xi, M.C. He and C.Y. Lin, Adsorption of antimony(V) on kaolinite as a  
146 function of pH, ionic strength and humic acid, *Environ. Earth. Sci.*, 2010, **60**, 715-  
147 722.
- 148 9 A. Sari, D. Çitak, M. Tuzen, Equilibrium, thermodynamic and kinetic studies on  
149 adsorption of Sb(III) from aqueous solution using low-cost natural diatomite, *Chem.*  
150 *Eng. J.*, 2010, **162**, 521-527.
- 151 10 F.C. Wu, F.H. Sun, S. Wu, Y.B. Yan and B.S. Xing, Removal of antimony(III)  
152 from aqueous solution by freshwater cyanobacteria *Microcystis* biomass, *Chem.*  
153 *Eng. J.*, 2012, **183**, 172-179
- 154 11 J. Li, X.D. Li, T. Hayat, A. Alsaedi and C.L. Chen, Screening of zirconium-based  
155 metal-organic frameworks for efficiently simultaneous removal of antimonite  
156 (Sb(III)) and antimonate (Sb(V)) from aqueous solution, *Acs. Sustain. Chem. Eng.*,  
157 2017, **5**, 11496-11503.
- 158 12 J.M. Luo, C.Z. Hu, X.Y. Meng, J. Crittenden, J.H. Qu, and P. Peng, Antimony  
159 removal from aqueous solution using novel  $\alpha$ -MnO<sub>2</sub> nanofibers: equilibrium,  
160 kinetic, and density functional theory studies, *Acs. Sustain. Chem. Eng.*, 2017, **5**,  
161 2255-2264.
- 162 13 J.P. Zou, H.L. Liu, J.M. Luo, Q.J. Xing, H.M. Du, X.H. Jiang, X.B. Luo, S.L. Luo,  
163 and S.L. L. Suib, Three-Dimensional reduced graphene oxide coupled with Mn<sub>3</sub>O<sub>4</sub>  
164 for highly efficient removal of Sb(III) and Sb(V) from water, *Acs. Appl. Mater.*  
165 *Interfaces*, 2016, **8**, 18140-18149.

- 166 14 M. Pena, X. Meng, G.P. Korfiatis and C. Jing, Adsorption mechanism of arsenic  
167 on nanocrystalline titanium dioxide, *Environ. Sci. Technol*, 2006, **40**, 1257-1262.
- 168 15 A.H. Chen, S.C. Liu, C.Y. Chen, C.Y. Chen, Comparative adsorption of Cu(II),  
169 Zn(II), and Pb(II) ions in aqueous solution on the crosslinked chitosan with  
170 epichlorohydrin. *J. Hazard. Mater*, 2008, **154**, 184-91.
- 171